



Research Article

Optical properties of synthesized Au/Ag Nanoparticles using 532 nm and 1064 nm pulsed laser ablation: effect of solution concentration

Shaghayegh AdibAmini¹ · Amir Hossein Sari¹  · Davoud Dorrnian¹

Received: 6 June 2022 / Accepted: 13 February 2023

Published online: 31 March 2023

© The Author(s) 2023 [OPEN](#)

Abstract

The primary objective of this experimental research is to introduce the capacity of laser irradiation into the synthesis of bimetallic nanoparticles from noble metals. Gold and silver nanoparticles are produced through the laser ablating gold and silver targets in distilled water. Originally, the samples are synthesized by using Nd:YAG laser with 1064 nm wavelength and 7 ns pulse width. Following this, solutions mixed with different volumetric ratios, are irradiated by the second harmonic of the said laser at 532 nm wavelength. The absorption peak of gold nanoparticles around 530 nm, is used to transfer the laser energy to nanoparticles and synthesize Au/Ag bimetallic nanoparticles. The wavelength and volumetric ratio of solutions are the experiment's variables. The bimetallic nanoparticles are characterized as follows: X-ray diffraction pattern, spectroscopy in the range of UV–Vis–NIR and IR, Photoluminescence spectrum, Dynamic light scattering, and Fourier transform infrared spectroscopy. Additionally, FE-SEM and TEM images are used to study the size and morphology of nanoparticles. One of the aims of the research is to investigate the effects of laser wavelength and different volumetric concentrations on the optical properties of Au/Ag bimetallic nanoparticles. On the other hand, the study revealed that silver concentration and laser wavelength in the synthesis of Au/Ag bimetallic nanoparticles with different structures, cause the formation of crystalline structure, growth of grain size, and therefore silver oxide reduction.

Article highlights

- Using two laser wavelengths and different silver concentrations, lead to the synthesis BNPs with different sizes and structures.
- High silver concentrations are limited due to oxidation and instability in the last sample.
- Synthesis of stable BNPs with controlled shell thickness is possible with the applied PLAL method.

Keywords Bimetallic nanoparticles (BNPs) · Pulsed laser ablation in liquid (PLAL) · Gold nanoparticles (AuNPs) · Silver nanoparticles (AgNPs)

Abbreviations

| | | | |
|-------|----------------------------|-------------------|-------------------------------------|
| NPs | Nanoparticles | AgNPs | Silver nanoparticles |
| BNPs | Bimetallic nanoparticles | PLAL | Pulsed laser ablation in liquid |
| MNPs | Monometallic nanoparticles | LSPR | Localized surface plasmon resonance |
| AuNPs | Gold nanoparticles | DIW | Distilled water |
| | | Ag ₂ O | Silver oxide |

✉ Amir Hossein Sari, sari@srbiau.ac.ir; amirsari@gmail.com; Shaghayegh AdibAmini, tulip.adib@gmail.com; Davoud Dorrnian, d.dorrnian@gmail.com | ¹Laser Lab., Plasma Physics Research Center, Science and Research Branch, Islamic Azad University, Tehran 1477893855, Iran.



SN Applied Sciences

(2023) 5:122

| <https://doi.org/10.1007/s42452-023-05310-1>

| | |
|-----------------|---|
| Ag ⁺ | Silver ions |
| XRD | X-ray diffraction pattern |
| UV-Vis | Ultraviolet-visible spectroscopy |
| FE-SEM | Field emission scanning electron microscopy |
| TEM | Tunneling electron microscopy |
| DLS | Dynamic light scanning |
| FT-IR | Fourier transform infrared spectroscopy |
| PL | Photoluminescence spectroscopy |

1 Introduction

In recent decades, the study and investigation of the different catalytic characteristics, surface plasma band energy and magnetic/electrical properties of bimetallic nanoparticles (BNPs), is become topics of interest. Comparison of BNPs with concentrated monometallic ones shows that the synthesis of BNPs in the form of alloy and core-shell can illustrate the unique characteristics of advanced linear and non-linear material, which are used in many fields of application, with significant catalytic and various electro-optical properties [1–4]. On the other hand, studying the non-linear behaviors of plasmonic nanoparticles (NPs) opens a new horizon of applications of noble NPs in the field of optics communication, information processing, heat transfer applications, solid-state lasers and biosensors [5, 6].

The synthesis of gold nanoparticles (AuNPs) as a 5d metal, is received remarkable attention due to their interesting applications in catalysis, non-linear optical devices, single electron tunneling and chemical sensing [7, 8]. Silver nanoparticles (AgNPs) as a 4d metal, are one of the most popular catalysts for oxidation and have higher electrical and thermal conductivities than other NPs. On the other hand, antibacterial properties are other significant characteristics of AgNPs [9–11]. Gold, silver and their composites at the nanoscale are received considerable attention, due to their application as a single electron transistor, gas sensor, detector of biomolecules and catalyst [12–16]. Synthesis of metal NPs in nano-dimensions and when interacting with external electromagnetic radiation, leading to electron confinement and localized surface plasmon resonance (LSPR), which will show their optical properties. The LSPR characteristic of NPs can be changed concerning its size, morphology, composition and crystallinity [17, 18]. Of course, it should be noted that spherical metallic NPs have negligible non-local effects [19]. Noble metals like silver and gold, exhibit a strong LSPR, due to the collective oscillation of the valence electrons in the half-filled s-subshells 5d¹ and 6s¹ [20]. Valence electrons of AgNPs when exposed to an external field are excited and show more plasmonic properties, compared to AuNPs [21]. In this way, its catalytic properties, magnetic and optical polarization,

electrical conductivity and antimicrobial properties are increased [22, 23].

So far, several methods for the synthesis of BNPs have been developed in recent decades; but, among them pulse laser ablation in liquid (PLAL) as a physical method is one of the best ways due to control the composition of the NPs and the ability to produce different structures (e.g. alloy, core-shell, ...) and compounds (e.g. oxides, bimetallic NPs) [24, 25]. On the other hand, PLAL technique prepares efficient NPs from many types of solids (metals and ceramics in different liquids), to facilitate the investigation of their photophysical and photochemical properties. The noticeable feature of PLAL technique compares to chemical synthesis, is the absence of uncontrolled biomolecules or other impurities [26, 27].

There are many methods for fabricating MNPs, including solvothermal [28], Photochemical method [29], plane wave pseudopotential method [30], replacement reaction method [31], catalytic reduction [32], spray pyrolysis [33], wet-chemical method [34], chemical reduction [12, 15], green synthesize [35–37], post-modification [38], electron beam deposition [23], Spark discharge [39], pulse laser deposition (PLD) [40–42] and PLAL [43–45]. In the following table (Table 1), a summary of the research carried out for the Au/Ag BNPs with different structures (alloy and core-shell), which are synthesized with the application of PLAL method in different solvents, is presented.

In this manuscript, the main harmonic of a high-frequency Nd:YAG laser is applied to forming gold and silver NPs individually; whereas, second harmonic irradiation with 532 nm wavelength, is used for the synthesis Au/Ag BNPs. The main goal is to characterize optical properties and to find the role of different wavelengths and ratio concentrations of AgNPs in the preparation of bimetallic systems with different structures (alloy and core-shell). The possibility of the formation of Au/Ag BNPs under this condition is another question of this research.

In the next section, we consider materials and methods applied to the experiment. Section 3, shows the characterization of monometallic and BNPs. In Sect. 4, we present the results and discussion. Section 5, illustrates the summary and conclusion. In the final sections, acknowledgment and author contribution are mentioned.

2 Materials and methods

Initially, gold and silver plates (99.9%) as ablation targets are ultrasonically cleaned by ethanol, acetone, and deionized water (DIW) for 10 min, respectively. The targets are put at the bottom of two containers with 200 mL of DIW. The thickness of DIW on target palates is 8 mm. Gold and silver targets are purchased from Sigma Aldrich Co. The

Table 1 Summarizes the optical characteristics of Au/Ag NPs in the typical literature in last ten years with different structures (alloy and core-shell) in distinct solvent

| Publication year | Structure | Synthesis method(s) | Kind of laser | Wavelength (nm) | Pulse duration (ns) | Repetition rate (Hz) | Pulse fluence (J/cm ²) | Solvent | Mean crystallite size (nm) | Morphology | Remarks |
|------------------|--|-----------------------------------|------------------|-----------------|---------------------|----------------------|------------------------------------|------------------------------------|---------------------------------|-------------------------------------|---|
| 2014 [46] | Monometallic AuNPs | PLAL | Nd:YAG | 1064 | 5 | 10 | 13.8, 20.5, 25.6 and 28.5 | Distilled water and ethanol | 70/6 | Spherical | Be Stable after 2 years |
| 2014 [47] | Monometallic Au and AgNPs | PLAL | Nd:YAG | 1064 | 7 | 10 | 1 and 3 | Distilled water | 2–41 | Spherical | Pure metal colloids can be prepared by this technique |
| 2015 [48] | Monometallic Au and AgNPs, alloy Ag-Au | PLAL | Nd:YAG | 1064 | 5 | 15 | 5 | Ethanol and methylene blue | 11–23 | Spherical | – |
| 2015 [45] | Alloy Au–Ag, Au core with Ag shell | PLAL | Nd:YAG | 1064 | 9 | 10 | 10 | Ethanol and PVP | Alloy: 17 core-shell: 25 | Spherical | Formation of nanoalloys with plasmon band tunable |
| 2015 [49] | Ag core with Au shell | PLAL | Nd:YAG | 1064 | 6–7 | 10 | 19.1 | Distilled water | 11–16 | Spherical | Tested the suitability of Ag@Au core-shell particles as substrates for SERS |
| 2016 [50] | Alloy Au/Ag, Ag core with Au shell | PLAL | Nd:YAG | 1064 | 6–7 | 10 | 19.1 | Distilled water/Au and Ag colloids | 9–12 | Spherical and nano-chain | Spiky nature of the distribution of energy states for both nanostructures |
| 2016 [51] | Monometallic Au and AgNPs, alloy Au–Ag | PLAL | Nd:YAG | 1064 532 | 8 | 10 | 18–20 | Ethanol | Au: 14.80 Ag: 8.47 alloy: 25.12 | Spherical | Without adding any surfactant |
| 2018 [40] | Monometallic Au and AgNPs, Ag/Au thin film | Thermal evaporation, PLD and PLAL | Nd:YAG | 355 | 15 | 10 | 1.5 and 5 | Distilled water | 2–20 | Spherical and nano-chain (nanowire) | Synthesis of NPs in different size |
| 2020 [52] | Alloy Au–Ag | PLAL | N/A | N/A | N/A | N/A | N/A | Distilled water | 10–20 | Multiply-twinned | Alloy NPs are formed homogeneously |
| 2021 [53] | Au core with Ag shell | PLAL and green synthesis | Nanosecond laser | 1064 | 7 | 10 | N/A | distilled water and PVA | Au: 2–35 Ag: 3–28 | Spherical | Increased in electrical conductivity |

Table 1 (continued)

| Publication year | Structure | Synthesis method(s) | Kind of laser | Wavelength (nm) | Pulse duration (ns) | Repetition rate (Hz) | Pulse fluence (J/cm ²) | Solvent | Mean crystallite size (nm) | Morphology | Remarks |
|------------------|-----------------------|---------------------|---------------|-----------------|---------------------|----------------------|------------------------------------|-----------------|----------------------------|------------|--|
| 2021 [4] | Au core with Ag shell | PLAL | Nd:YAG | 1064 532 | 7 | 10 | 1.8 | Distilled water | 5–30 | Spherical | Nonlinearity response of the core–shell structure This structure is non-toxic |
| 2021 [54] | Ag core with Au shell | PLAL | Nd:YAG | 1064 532 | 10 | 1 to 6 | 0.2 to 1 | Distilled water | 20–30 | Spherical | |

procedure for PLAL method is as follows: High-energy laser radiation with 1064 nm wavelength, is focused on the individual gold and silver target immersed in the liquid and during the ablation process plasma plume is formed and condensed around the focus point. Finally, NPs are synthesized and suspended in the liquid to form nanocolloids [55]. Following this, the post-laser irradiation of mixed solutions is carried out at a wavelength of 532 nm with 5000 laser pulses. This second harmonic of laser is selected due to the intensive plasmon absorption band of AuNPs in the vicinity of 524 nm, which results in increasing the chance of bimetallic formation from gold and silver NPs [44]. On the other hand, the 532 nm wavelength of the laser, is more effectively absorbed by the plasma plume during the ablation and the process of forming BNPs is done with higher quality [26].

In this research, using the Gaussian beam equations, the spot size of the laser on the surface of the target is calculated to be about 30 μm. Target is irradiated with 5000 pulses of the fundamental wavelength of a pulsed Nd:YAG laser (Quantel, model Brilliant B) of 1064 nm wavelength, operating at 10 Hz repetition rate and 7 ns pulse width with a fluence of 0.5 J/cm². The Laser beam 6 mm in diameter, is focused on the surface of the target using a 10 cm focal length convex lens. Meanwhile, it should be noted that the continuous laser with a lower heating rate than the pulsed laser, synthesizes NPs with the desired morphology and greater accuracy [55].

In this case, we are able to distinguish between our work and other research. In most of the articles that have been done for the synthesis of MNPs and BNPs by the PLAL method, the NPs have been synthesized with the first harmonic (1064 nm) of the laser. In other investigations, besides the use of the first and second harmonics (532 nm) laser parameters such as repetition rate, pulse fluence and pulse duration are variable [4, 51, 54]. In the research conducted by Ayman et.al. the selected pulse fluence (1.8 J/cm²) exceeds our selected parameter (0.5 J/cm²) [4] (Table 1).

The noncolloidal solutions of gold and silver obtained as demonstrated in Fig. 3 are mixed in different volumes. These ratios are AgAu₂ (12.5 mL of Ag mixed with 25 mL of Au nano-colloidal solution—s1), AgAu (25 mL of Ag mixed with 25 mL of Au—s2), Ag_{1.5}Au (37.5 mL of Ag mixed with 25 mL of Au—s3), and Ag₂Au (50 mL of Ag mixed with 25 mL of Au—s4) (see Table. 2). Gold and silver liquid NPs, appeared in specific colours that indicate the plasmonic excitement of noble metal when forming NPs [20, 56] (Fig. 1a). During the initial harmonic irradiation (1064 nm), the colour of gold and silver solution, step-by-step switches from light red to dark violet and light yellow to dark brown, respectively (Fig. 1b) [20, 57, 58]. By using post-irradiation (532 nm), the colour of Au/Ag

Table 2 Parameters of prepared samples

| Sample (#) | s1 | s2 | s3 | s4 | s5 | s6 |
|-----------------------------|---------|-------|---------|-------|-------|-------|
| Ag/Au volumetric ratio (mL) | 12.5/25 | 25/25 | 37.5/25 | 50/25 | 0/100 | 100/0 |

colloidal NPs with a growing ratio concentration of AgNPs, changes from dark brown to light brown (Fig. 1c). Changes in colours, is occurred because of relativistic effects and increasing the energy of the 5d orbital and decreasing the energy of the 6s orbital in gold. These effects result in a shift absorption peak from the ultraviolet region to the lower. In bulk silver, relativistic effects are smaller than in gold, and the distance from 4d to 5s is much larger; as a result, transitions are seen in the ultraviolet region [20, 59]. Synthesis conditions may be influenced by the LSPR properties of plasmon metals [60]. The synthesized BNPs did not precipitate and remained in colour for two years. A schematic of the ablation process appears in Fig. 2.

3 Characterization of Au, Ag and Au/Ag nanoparticles

A variety of analytical techniques are applied for the characterization of NPs. The optical spectra of colloidal solutions are characterized with a UV–Vis spectrophotometer (T80 UV–Vis Spectrometer/PG Instrument Ltd). A Transmission Electron Microscope (TEM; Zeiss-EM10C-80 kV), is used to determine the size, shape, and distribution of NPs. This experiment is performed by placing a drop of the concentrated suspension on a carbon-coated grid Cu Mesh 300 and kept completely dry at room temperature. The crystal structure characterization is done by the X-ray diffraction (XRD) technique. The concentrated suspensions, are dropped on a silicon substrate and dried for ten days for XRD measurement. The surface morphology of the NPs is examined by field emission scanning electron microscope (FE-SEM, HITACHI S-4160 instrument). The dynamic light scattering (DLS) technique, is used to obtain the size and distribution of NPs by measuring a hydrodynamic diameter using the MALVERN ZETASIZER device. The PERKIN ROMER PL facility obtained the photoluminescence (PL) properties of Au/Ag colloids. The dried sample films are characterized by Fourier transform infrared (FT-IR) spectroscopy (Thermo Nicolet, Nexus 870).

4 Results and discussion

4.1 X-ray diffraction (XRD) studies

The XRD patterns of the individual gold and silver beside Au/Ag BNPs with varying silver ratio concentration, are

presented in Fig. 3. In the XRD pattern of all samples, a peak of X-ray photons diffracted from silicon substrate is seen at 68.9°. According to XRD results in Fig. 3, the detected phases are gold (PDF cards No. 01-087-0718), silver (PDF cards No. 01-089-3697), and Au/Ag (PDF cards No. 03-065-8424), respectively. It can be seen four diffraction peaks are detected at (111), (200), (220), and (311) planes for fcc structure of AuNPs. The following, four diffraction peaks are observed at (111), (200), (220), and (311) planes for AgNPs with fcc Bragg lattice. Moreover, Au/Ag BNPs, have a similar XRD structure as bulk gold and silver NPs and have four diffraction peaks at (111), (200), (220), and (311) planes, respectively (see Table. 3). In consequences, the bimetallic system has analogous fcc structures, same lattice constants (gold 4.0783 Å and silver 4.0862 Å) and similar atomic radius (gold = 1.74, silver = 1.65), as a monometallic plasmonic gold and silver NPs [34]. Thus, the XRD diffraction peak of gold and silver are close together, and XRD analysis cannot be the ethical option to definitively prove the existence of bimetallic structure, which is in good agreement with this paper [21, 61, 62]. Due to the detection of sharp peaks in all bimetallic samples (Fig. 3), it is possible to confirm the synthesis of crystalline nano-structures and demonstrate that amorphous structures are not formed [61, 63].

Silver oxide (Ag₂O) in s4 and s6, is detected in (111) plane at 32.9° with a significant peak (PDF card No. 03-065-6811) (see Table. 4). Standard oxidation states of silver, are + 1 (Ag (I), the most stable state), + 2 (Ag (II), highly oxidation), and very rarely + 3 (Ag (III), extreme oxidation) [64]. There is a volumetric threshold ratio during the ablation process at which, the formation of Ag₂O in DIW starts. In s1 to s3, the concentration ratio for AgNPs is below the volumetric threshold and Ag₂O is not formed. The following, crossing the threshold in s4 and also s6, Ag₂O appears. The AuNPs are the best option for the synthesis of a stable bimetallic structure with AgNPs and are located as a nucleus for controlling the reduction of silver ions (Ag⁺) [12, 65]. The Au–O is less ionic than Ag–O structure since gold has a much larger electronegativity (+ 2.54 eV) than silver (+ 1.93 eV) [30, 47].

Crystal structure, phase purity, and crystalline size of prepared gold and silver NPs and Au/Ag BNPs, are confirmed by Scherrer's formula (Eq. 1).

$$d = \frac{K\lambda}{\beta \cos \theta} \quad (1)$$

In this equation: k (dimensionless shape factor) is $0.89 < k < 1$; λ (wavelength of X-rays) equals 1.5406 Å; β is

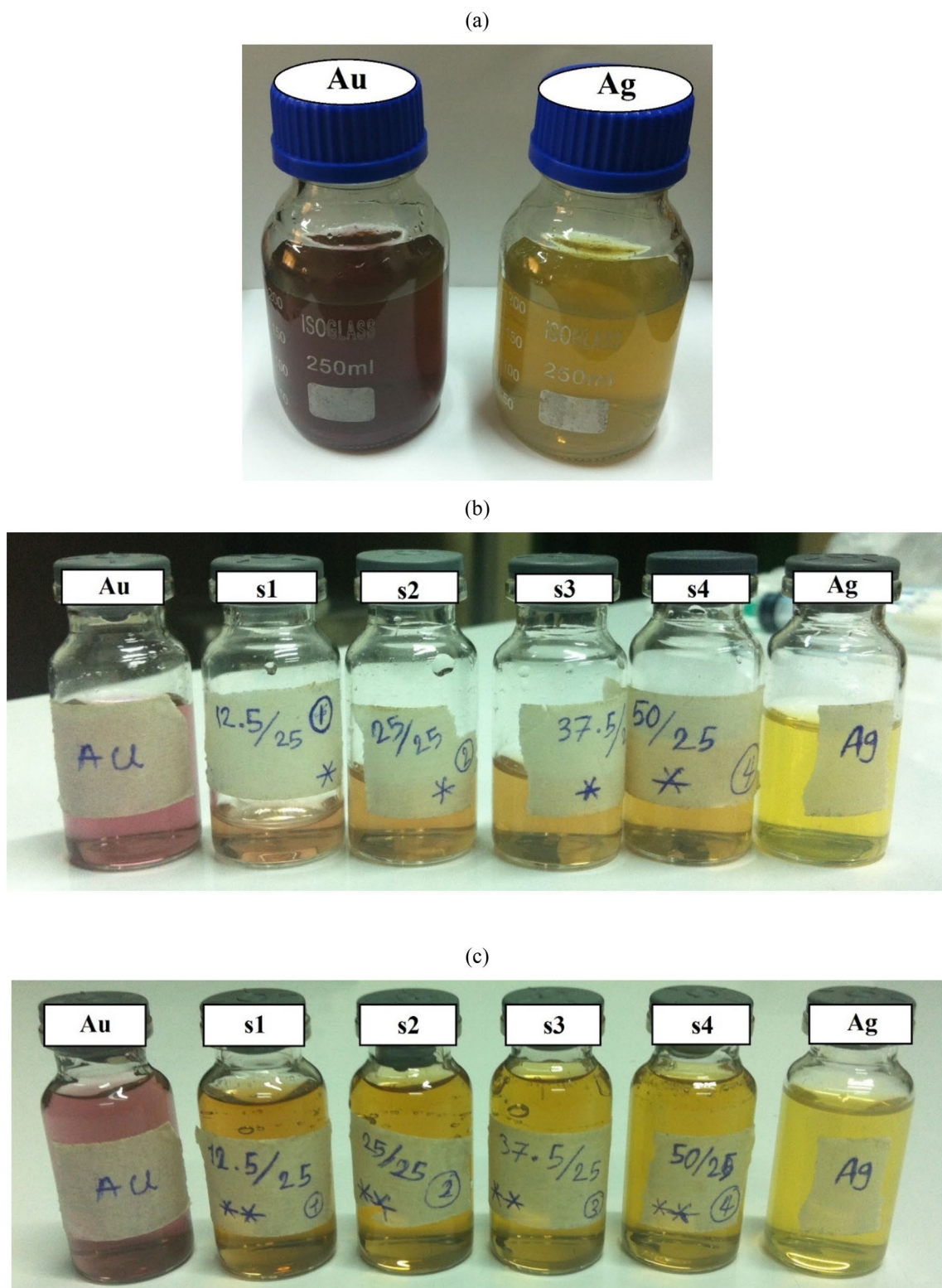


Fig. 1 Gold and silver nanoparticles formatted by irradiation of 1064 nm wavelength **a**, Au and AgNPs suspensions beside their mixtures before green laser irradiation **b** and Au/Ag BNPs with different volumetric ratio after green laser irradiation **c**

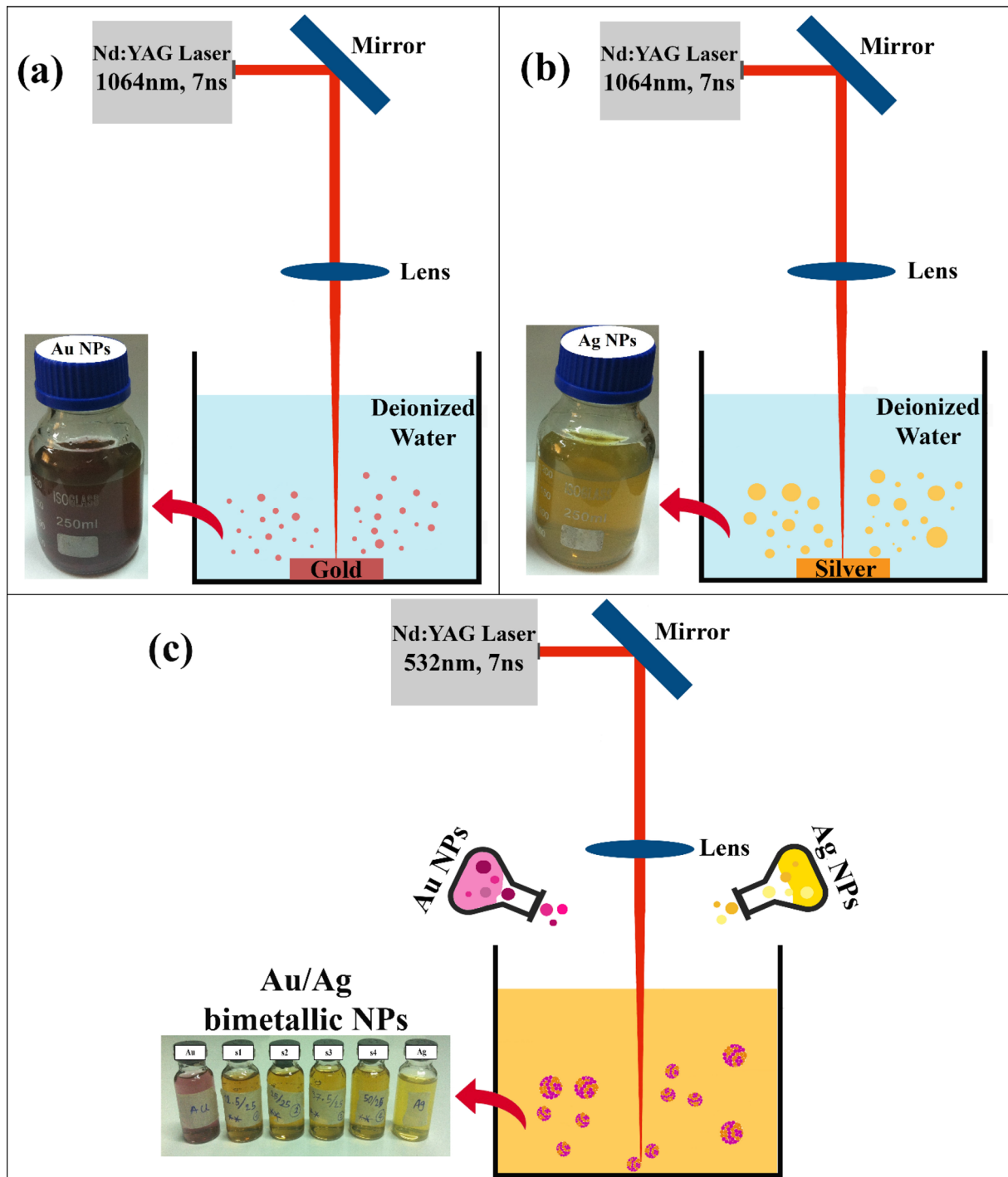


Fig. 2 Schematic of the laser ablation process. Show synthesize Au and AgNPs individually by first harmonic irradiation (1064 nm) **a** and **b** and illustrate formatting Au/Ag BNPs by green laser irradiation (532 nm) **c**

the line broadening at full width at half maximum (FWHM) in radius; θ is the Bragg's angle; and d is the average crystalline size of nanoparticles (which may be smaller or equal to the grain size and particle size). The most important peak of diffraction belongs to the (111) plane and shows that gold and silver have pure crystalline fcc structure.

The peak of the crystallite plane (111) in BNPs, is more intense than the other planes and suggests that the (111) plane is the predominant orientation [30]. Moreover, by increasing the concentration ratio of AgNPs, the width of the peak belonging to crystallite planes of (111) and (311) declined. The decrease in the width of the peak is related

Fig. 3 X-ray diffraction pattern of Au and AgNPs beside synthesized Ag/Au BNPs

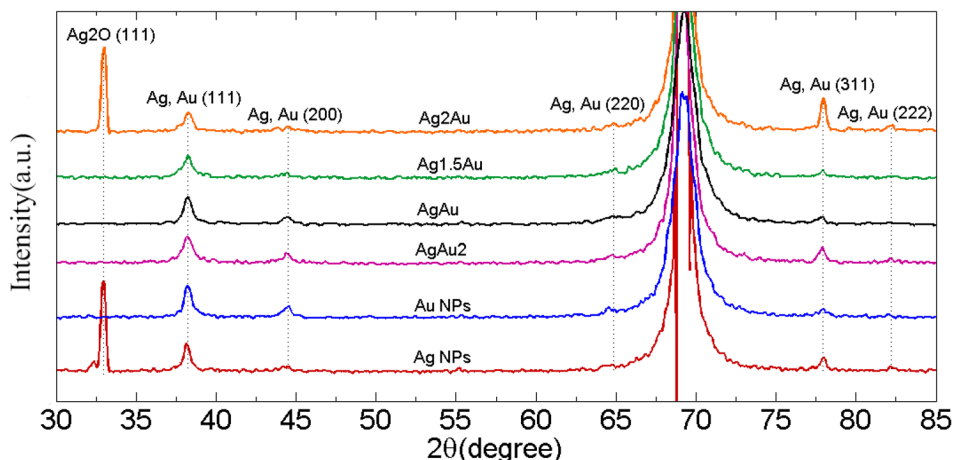


Table 3 Summary of XRD data for monometallic gold and silver NPs and bimetallic structures

| Sample (#) | FWHM | 2θ | Crystallite size (nm) | Reference pattern |
|------------|--------|-------|-----------------------|-------------------|
| s1 | 0.5510 | 38.18 | 16 | 03-065-8424 |
| s2 | 0.3936 | 33.10 | 22 | 03-065-8424 |
| s3 | 0.6298 | 38.26 | 28 | 03-065-8424 |
| s4 | 0.3936 | 38.19 | 32 | 03-065-8424 |
| s5 | 0.3936 | 38.15 | 22 | 01-087-0718 |
| s6 | 0.4723 | 32.95 | 33 | 01-089-3697 |

Table 4 Summary of XRD data of recognized Ag₂O in s4 and s6

| Sample (#) | FWHM | 2θ | Crystallite size | Reference pattern |
|------------|--------|-------|------------------|-------------------|
| s4 | 0.3936 | 38.19 | 32 | 03-065-6811 |
| s6 | 0.4723 | 32.95 | 33 | 03-065-6811 |

to Debye–Scherrer’s equation and the crystallite size. With an increasing volumetric ratio of AgNPs, the size of BNPs is increased. Likewise, the mean crystallite size of s1-s4 is recognized at 16 nm, 22 nm, 28 nm, and 32 nm respectively. In addition, the mean crystallite size of s5 and s6 is 22–33 nm, respectively.

In this research, bimetallic systems based on synthesis conditions, have been synthesized in different structures (alloy and core–shell). The alloy structure of Au/Ag bimetallic system (s1), is observed due to the galvanic replacement reaction between the noble Au and AgNPs interface and can be proven through UV–Vis analysis and TEM images [21]. Moreover, as the silver concentration increases the probability of galvanic replacement reaction in the samples (s2-s4) is reduced and core–shell structures are formed. In s2-s4, silver atoms attach to surface AuNPs present in the ablation medium and Au_{core}/

Ag_{shell} NPs are synthesized [32, 66]. On the other hand, based on Moiré model, because of overlap between core and shell, the core–shell structure is formed [67]. According to the Moiré model, the synthesized BNPs have the same crystalline structure and their Bragg planes rotate at a small angle relative to each other [21]. Core–shell structures, the difference in the plane interval of the shell and core leads to the Moiré model [68]. Gold NPs due to their spherical symmetry are chosen as the core for the formation of the Au_{core}/Ag_{shell} BNPs [45]. Therefore, due to the aforementioned similarities in the atomic structure of Au and AgNPs and the high plasmon excitation efficiency of AgNPs relative to AuNPs, the synthesized core–shell structure has no homogeneous contrast and the unequivocal core–shell structure is present in the samples (s2-s4) [21]. The following, core–shell structure and boundary between the Au_{core}/Ag_{shell}, have been distinguished with the lighter exterior and darker center, by the TEM images and the UV–Vis spectrum.

4.2 UV–Vis spectrophotometry

Figure 4 presents the results of absorption spectra from nanocolloidal samples, which illustrate the plasmonic characteristics of monometallic NPs and bimetallic structures. The special ability of gold and silver NPs to absorb incident electromagnetic radiation due to the LSPR leads to an interface between noble NPs, their dielectric surrounding, and also the collective oscillation of conduction electrons at the surface of particles [69, 70]. The LSPR effect may lead to the enhancement of the local electric field around the surface of plasmonic gold and silver NPs [66].

One of the predominant characteristics of plasmonic NPs is the organized multipolar LSPR (dipolar, quadrupolar, octupolar, and hexadecapolar modes), which significantly depends on the shape, size and structure [71].

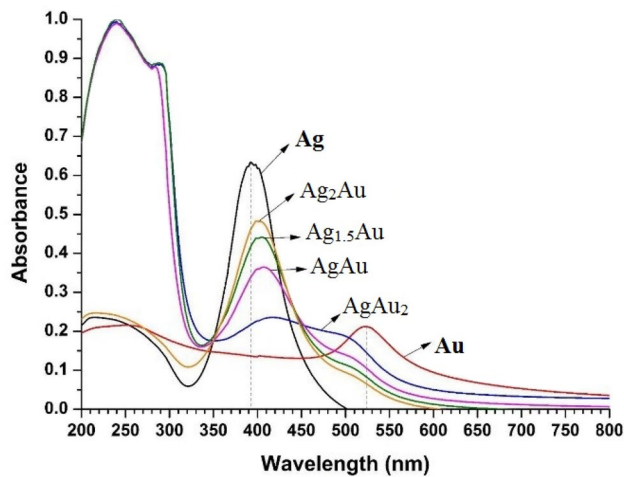


Fig. 4 UV-Vis-NIR absorbance spectrum of Au and AgNPs beside Au/Ag BNPs after green laser irradiation

Based on the UV-Vis graph, the peak at 523 nm is relative to dipolar LSPR mode absorption of the AuNPs. Other peaks observed at 260–217 nm are also, because of the higher-order quadrupole absorption in noble gold NPs [32, 44, 72]. Peaks belonging to AuNPs in the ultraviolet region (below 400 nm), are associated with electron transfer from the ligand to the metallic band ($\pi \rightarrow \sigma^*$) [73]. Detection of peaks in the visible and ultraviolet regions indicates the formation of AuNPs [21]. The other peak observed at 392 nm is due to the dipole LSPR absorption band of the AgNPs [74]. Around 210 nm, because of transition $\pi \rightarrow \sigma^*$ the quadrupole LSPR is also confirmed. All these peaks belong to AgNPs and are represented within the formation of silver NPs. On the other hand, the peaks of single LSPR in the dipolar mode for Au and AgNPs, show that the synthesized NPs have an almost spherical morphology. The intensity of the dipolar peaks with a growing concentration of AgNPs is incremented. Similarly, the FWHM according to the volumetric ratio of the AgNPs, is reduced. In this way, the size of BNPs is increased [75].

The four dipole plasmon absorption bands emerged between the LSPR peaks of monometallic Au and AgNPs (417 nm, 408 nm, 400 nm, 397 nm), are illustrated the Au and the AgNPs are overlapped together by plasmon decoupling and finally, the bimetallic system is formed. In the s1, in the visible range, two distinct peaks have appeared in the vicinity of 500 nm and 417 nm, representing the dumbbell NPs overlapped by an L-length dimer. As the dumbbell length decreases, the bimetallic structures experience a blueshift and a single peak will be observed [76]. This change can also be seen in TEM images as with the increase in silver concentration. The following, the BNPs are placed next to one another with $L \rightarrow 0$ and NPs with dumbbell structure, will disappear. The significant

blueshift of the LSPR band belongs to the bimetallic structure was also interpreted because of the damping of the LSPR gold as a core, by the surface of the Ag atoms as a shell and regards the formation of the core-shell structure [77, 78]. On the basis of the standards defined for plasmonic NPs of gold and silver, red-shift should be observed in the bimetallic structures of both elements. But in some cases, during overlapping of NPs the observed blueshift indicates the formation of the core-shell structure [21, 76].

As can be seen from the Fig. 4, the peak of s1 is shifted to shorter wavelengths (blueshift), but its height has not changed, and it is the same as the height of the peak belonging to AuNPs. On the other hand, it is likely that the s1 probably has an alloy structure. In the following, the other samples (s2-s4) not only have blueshift but the height of the peaks also is changed and that may likely have core-shell structures and that is confirmed by TEM results [4, 45, 79]. On the other hand, it can be said that with an increasing concentration ratio of AgNPs, it sees an increase in the size of the $Au_{\text{core}}/Ag_{\text{shell}}$ NPs, because of numerous interfacial couplings between gold and silver NPs. Similar results are reported in these papers [44, 79, 80]. Finally, other peaks are observed in the range of 210–240 nm of the ultraviolet region, also belonging to the quadrupolar LSPR band and derived from the dipolar oscillation of BNPs [76, 81].

Generally, the appearance of the quadrupole mode in all samples is because of the retardation, energy-shifting, radiation scattering, and size effect of the BNPs (above the size of 10–65 nm) [42, 71]. However, it should be noted that the defined size is related to the hydrodynamic radius of BNPs as determined by the DLS analysis [21]. The energy-shifting effect occurs when the size of NPs is not insignificant compared to the incident wavelength [71]. Of course, the radiation scattering effect is also effective for revealing the dipole LSPR mode. By increasing the size of NPs and revealing the quadrupole mode at low wavelengths, the communication of the surface charge on the plasmonic metals with the environmental dielectric is avoided. On the other hand, due to the emerging dipolar LSPR mode, plasmonic BNPs come into contact with the dielectric function related to the environment. Therefore, any small area on the surface of the metal acts as planar bulk metal. These conditions can be further investigated by examining the surface charge distribution and the electric field around BNPs [82]. During the ablation process, the LSPR bandwidth of silver NPs is lower than the core-shell structures. On the other hand, increasing the LSPR bandwidth of gold NPs leads to an increase in the dielectric function of the AuNPs [42].

In a noble metal, due to the high density of energy and remarkable separation in energy levels within the half-filled conduction band, LSPR appears at divided

energies from any interband transitions. As a result, AgNPs produce stronger LSPR and catalytic properties compared to gold NPs [77, 78]. In the ultraviolet region (above 400 nm), due to interband transition among the 5sp conduction-band and 4d band of AgNPs, a sharp absorption peak appeared (especially in s1–s3) [20, 42, 83]. Also, due to a hydrodynamic radius greater than 65 nm, the quadrupole mode has a greater role in the formation of bimetallic system and the intensity of the peaks in the ultraviolet region is higher compared to the visible region [21].

During the synthesis of BNPs by ablation, as long as silver NPs as a shell of bimetallic structure remains stable during growth and do not react with biomolecules in the environment, BNPs will not oxidized (This result is true for s1 to s3). When the molar amount of silver crosses the concentration threshold, the entropy of the bimetallic system is increased and the system reaches instability. Thus, due to the instability of the surface charge and the strong reaction of silver atoms with oxygen in the environment leading to, the s4 it will be oxidized and it will be highly reactive [21]. In the s4 where the concentration of silver NPs has exceeded the threshold concentration ratio, the silver is oxidized and the effect of interband transitions among gold and silver NPs is reduced. Growth in the concentration of AgNPs at s4, leading to a decline of the absorption peak in the ultraviolet region and the effectiveness of the quadrupole mode, is less observed in the oxidized bimetallic structure. On the other hand, the dipolar mode is shown with a more intense peak. The spectrum of s4 has shown an intense absorption peak at the wavelength region of 404 nm to confirm the synthesis of Ag₂O NPs, due to electronic transitions from the valence bond to the conduction bond [51]. In the sample of pure silver (s6), we also encountered Ag₂O compound.

The optical properties of core–shell BNPs are of great interest and by changing the thickness of the shell, the catalytic properties of the bimetallic system can be manipulated [84, 85]. In the bimetallic samples, an increase in the concentration of AgNPs was observed, which leads to an enhancement in the surface charge distribution and the electric field around BNPs. In this condition, there could be more functional groups on the surface of the silver atoms as a shell for the more chemical reactions with biomolecules in the environment, and finally may be modified the catalytic efficiency. Due to the characteristics of the ablation method and the stronger electronic effect between core and shell (without adding surfactants and metal ions), after crossing the saturation threshold, the s4 and s6 do not have a non-linear behavior and react with the oxygen in the environment and are oxidized [12, 86]. In general, samples with core–shell structures have more catalytic properties compared to alloy structures and monometallic

NPs [24, 87, 88]. Chemical analysis is required to accurately check the catalytic properties.

The bandgap energies of BNPs, are estimated from the transmission spectrum by using the Tauc equation to describe the PL spectrum and properties influencing the photocatalytic performance of BNPs. The influence of nanocrystal size on the electronic structure of semiconducting BNP is demonstrated by the enhancement of bandgap energy and a decrease in particle size. In other words, this effect is called the quantum confinement effect. Based on the Tauc equation (Eq. 2):

$$\alpha hv = B \left(hv - E_g \right)^n \quad (2)$$

where α is the absorption coefficient, $h\nu$ is the photon energy, E_g refers to the bandgap energy, and B is a factor that depends on the transition probability. The index m is relative to the distribution of the density of states. The index n has different values like 1/2, 3/2, and 2 more depending on whether the transition is direct or indirect and allowed or forbidden, respectively. Taking $n = 1/2$ corresponds to direct allowed transitions of Au/Ag BNPs semiconductor. Corresponding band gap values of s4 and s6 could be identified according to this equation (Eq. 3):

$$E_g = \frac{1240}{\lambda_g} \quad (3)$$

where E_g is the semiconductor's bandgap and λ_g is the threshold wavelength of the corresponding absorbance edge. The bandgap energy of s4 and s6 as a semiconductor strongly depends on their size and morphology. Therefore, the values of the direct bandgap energies of s4 and s6 are observed in 2.50–2.73 eV, respectively (Fig. 5). For synthesizing Ag₂O, S.P. Vinay et al. show that the bandgap energy is found around ~2.74 eV [11, 84]. This result illustrates excellent catalytic properties for Ag₂O, due to its sensitivity to absorbing a photon with a wide bandgap

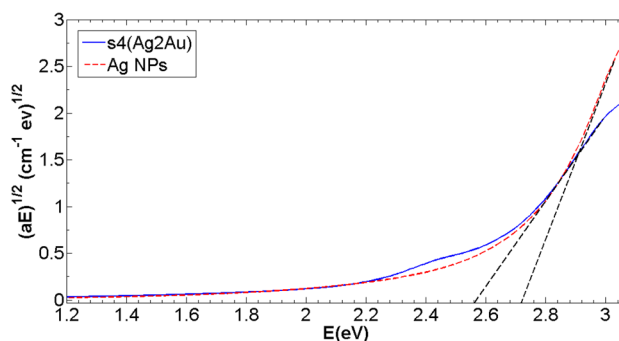


Fig. 5 Tauc plots to extract the bandgap energy of Ag₂O in s4 (blue line) and Ag NPs (dashed red line) as a semiconductor

energy [84]. The bandgap energy of s4 is decreased compared to s6 and indicates the size of produced Au/Ag BNPs in s4, is increased.

4.3 Morphology studies

4.3.1 Electron microscope studies (TEM and FE-SEM)

A transmission electron microscope (TEM) is regulated to obtain the micrograph of the NPs and demonstrate the spherical morphology of bulk gold, silver, and BNPs. Field emission scanning electron microscope (FE-SEM) analysis estimates the structure and morphology of the fabricated NPs. The spherical morphology also confirms the results of the TEM analysis. TEM and FE-SEM images show the average size and morphology of bulk gold and silver NPs (Figs. 6 and 7). The structure of BNPs according to the two-step synthesis method and medium conditions, can be divided into three branches: including dumbbell, core-shell, and alloy structures as illustrated in Fig. 8. With regard to TEM images (Figs. 9 and 10), it is clear that the atoms of Au are concentrated in the center,

while the atoms of Ag are located around the gold atom. These phenomena illustrate the synthesis of a quasi-homogeneous core-shell structure [21]. The synthesized BNPs system indicates random homogeneous shapes as a core-shell with the same atomic lattice. Similarly, the final morphology of nanostructures is dependent on forces, including the strength of the bond between Au/Ag BNPs [89]. The cause of the high atomic number in gold as against silver ($Z_{\text{Au}} = 79 > Z_{\text{Ag}} = 47$), attenuation of electrons from gold and silver atoms. In addition, high contrast of emission light from the surface of gold atoms, can be recorded in the spherical form of NPs with dark and light spots [31, 57, 58, 78]. Silver NPs are larger than gold NPs and the average size of Au/Ag BNPs increases by a different volumetric fraction from silver NPs. According to the report of Amikura and his colleagues, spherical NPs are formed in environments with a significant rate of oxygen, which is proved by SEM and TEM analysis [90]. In oxidized samples (s4 and s6), nano-scale particles with a fewer dumbbell structures are formed and more rounded edges are defined.

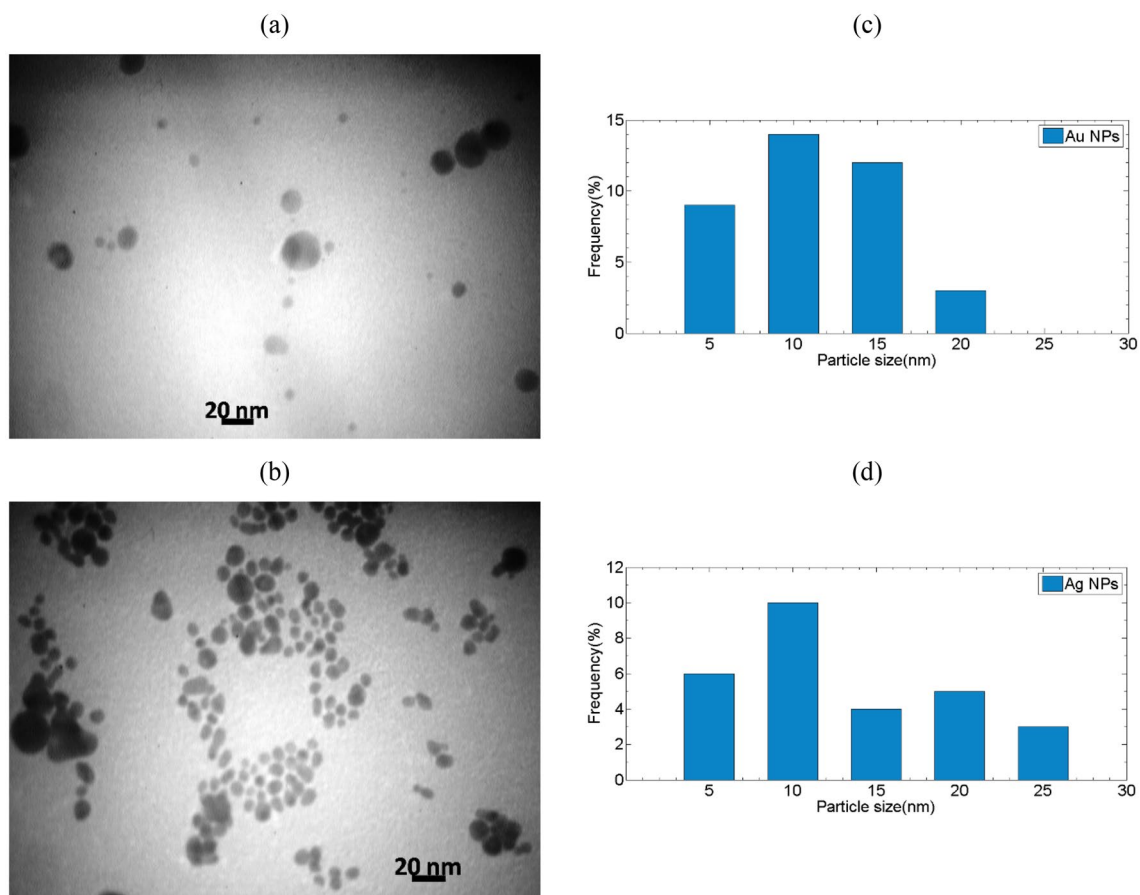


Fig. 6 Representative TEM images of AuNPs **a** and AgNPs **b**. **c** and **d** histogram showing the average size of AuNPs and AgNPs, respectively

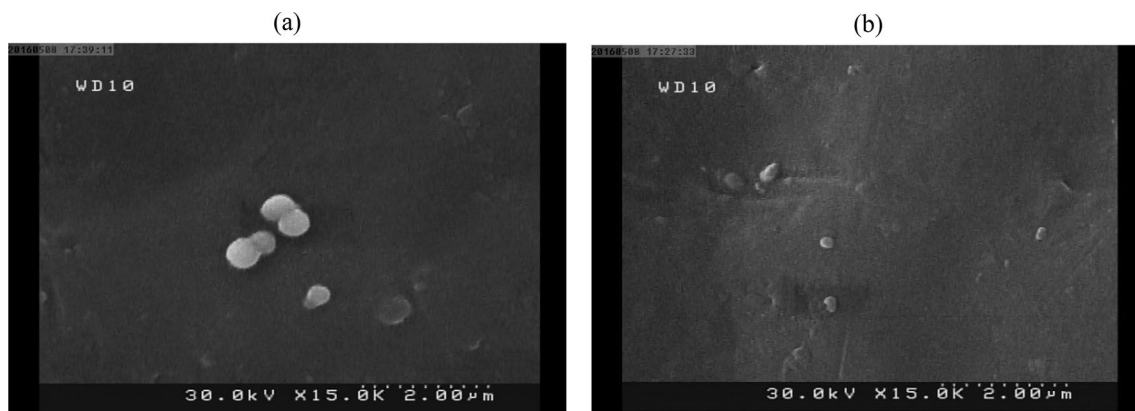


Fig. 7 SEM micrographs of Au and AgNPs samples dried on aluminum foil

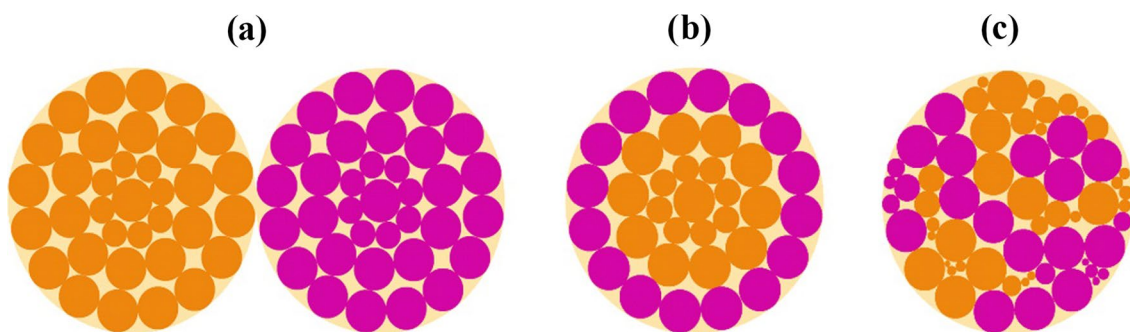


Fig. 8 Schematic of BNPs structure depend on two-step synthesis method and medium condition. Dumbbell **a**, core-shell **b**, and alloy **c** structures

4.3.2 DLS studies

The size distribution of BNPs reflected in the hydrodynamic diameter is determined by dynamic light scattering (DLS) with the drop-up colloidal-solution concentration of gold and silver NPs. By raising the silver concentration, the hydrodynamic radius of Au/Ag BNPs and their abundance with the bigger size amplifies is increased (Fig. 11). The hydrodynamic radius of gold and silver NPs is measured at 78.7–90.6 nm, respectively. Following the results of the bimetallic system the hydrodynamic radius of BNPs are in the vicinity of 92.4 nm, 100.2 nm, 105.4 nm, and 107.1 nm, respectively, and it is much larger than the size observed in TEM, FE-SEM and crystallite size obtained from XRD results (Fig. 12). As mentioned in the UV-Vis analysis, by increasing the silver concentration and hydrodynamic radius, the retardation effects are shown more effective and the quadrupolar LSPR mode is observed under 400 nm [42, 71]. When the size of NPs is increased, the quadrupolar mode also is appeared in lower wavelengths [21].

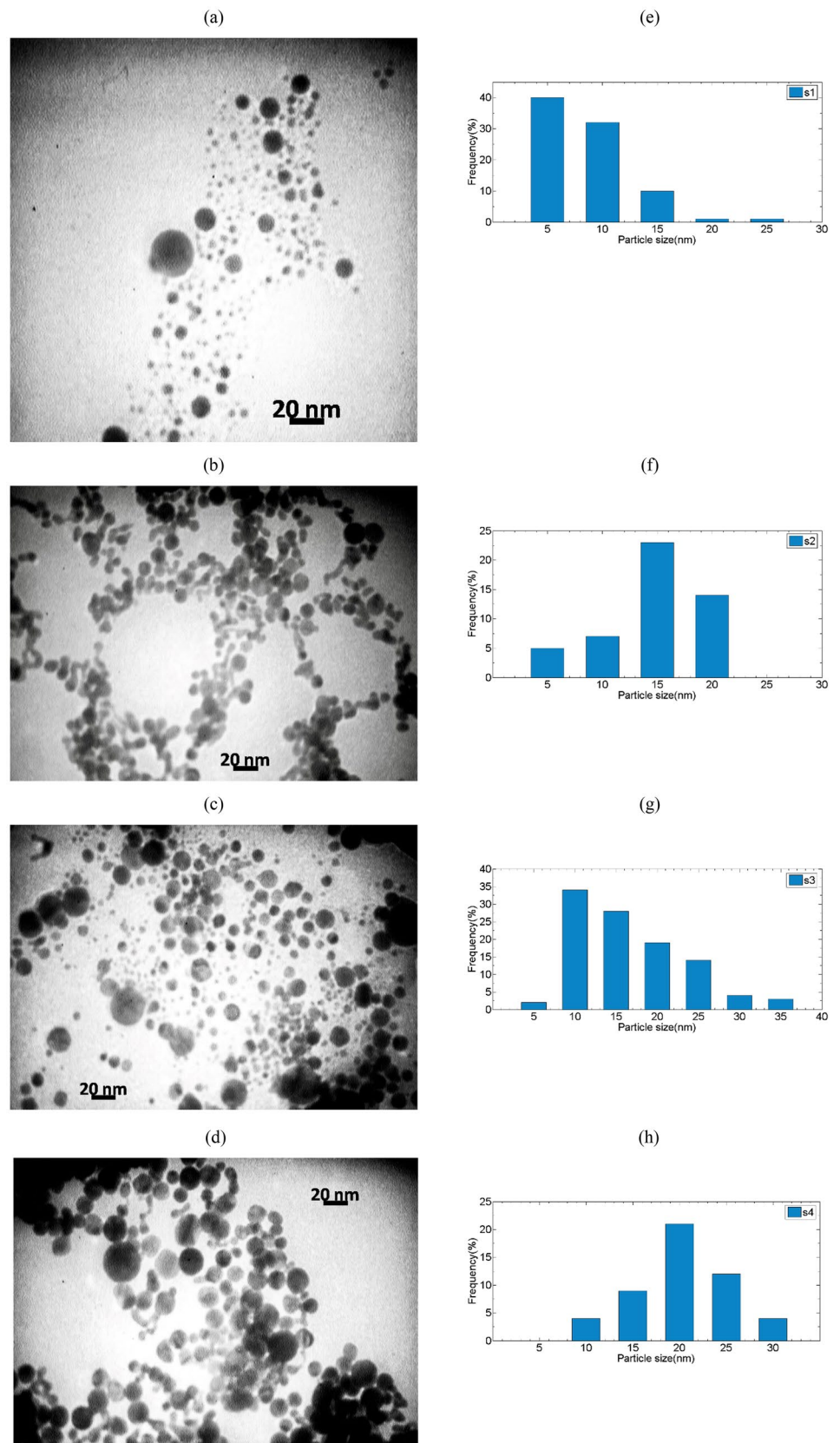
The average particle sizes of samples obtained from XRD, TEM, and FE-SEM images are shown in Table 5. DLS

estimates compared to other analyses are higher, due to the agglomeration of Au/Ag BNPs in liquid media during the ablation by the fusion redispersion process [21, 52, 91]. The overlapping of electron-hole wavefunctions with the enhancement of the excitonic energy indicates how the particle behaves in a liquid based on NPs diffusion [92, 93]. Another reason for the difference between TEM and DLS measures, is the core and shell have more interparticle attraction randomly because of the van der Waals during the dynamic conditions. Other objectives include the following plasmonic interactions, as well as interpositional repulsion as a result of electrostatic and steric interactions are other purposes [94]. A Summary of data about the hydrodynamic radius of Au/Ag BNPs is reported in Table 6.

4.4 FT-IR studies

Fourier transform infrared spectroscopy (FT-IR) is offered to investigate the specific surface chemistries and possible active molecules responsible for the reduction and vibrations of atoms within a molecule of liquid gold, silver, and Au/Ag BNPs. For this reason, a spectrophotometer

Fig. 9 Representative TEM images of AgAu₂ **a**, AgAu **b**, Ag_{1.5}Au **c** and Ag₂Au **d**. **e** to **h** histogram showing the average size of s1-s4 NPs, respectively



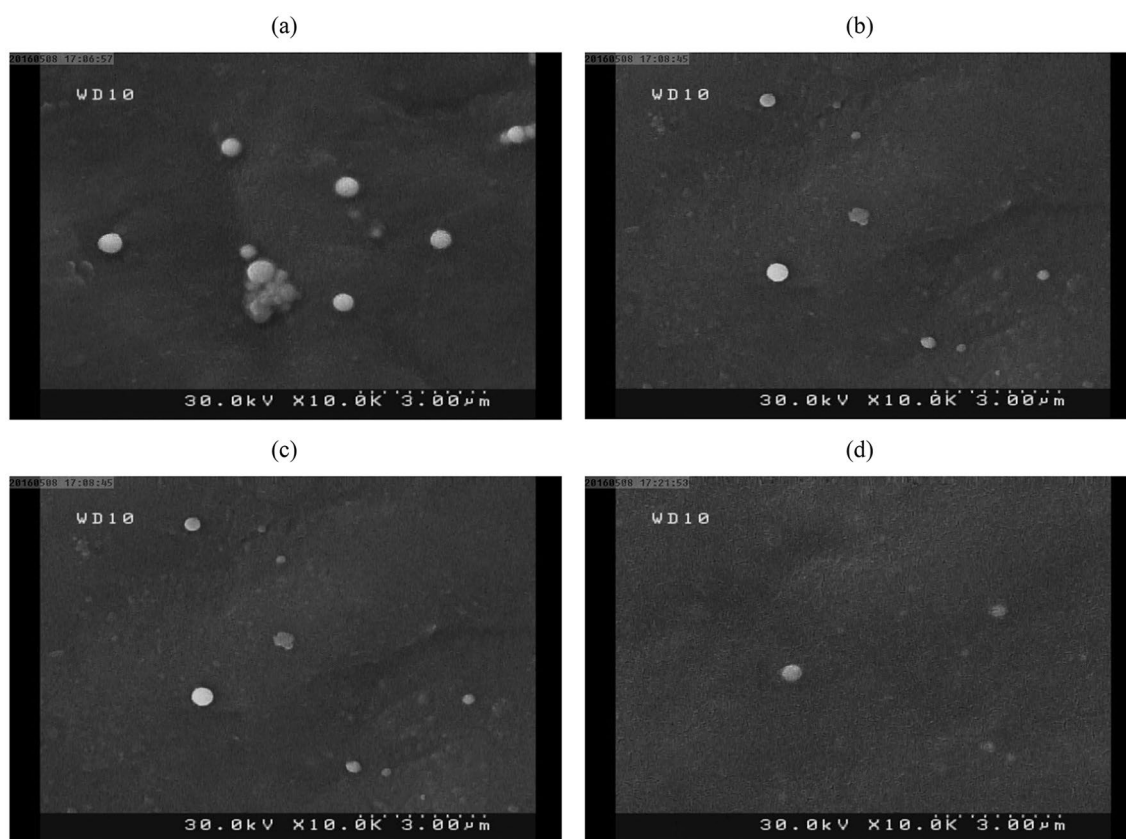


Fig. 10 SEM micrographs of Au/Ag BNPs samples dried on aluminum foil

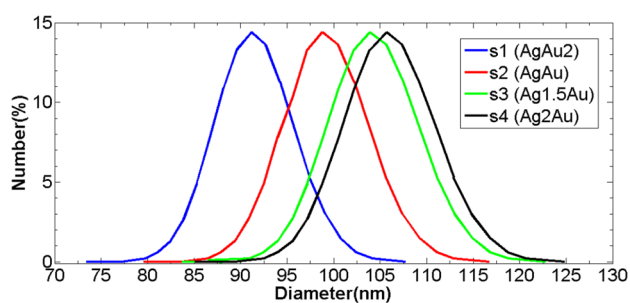


Fig. 11 The size of NPs obtained from DLS samples

applied in the range between 400 and 4000 cm^{-1} for all samples, used in this research, and the fingerprint region (500–1500 cm^{-1}) revealed specific properties of synthesized NPs [7]. Attention to Fig. 13a, shows that Au and AgNPs have peaks with different intensities. On the other hand, the peaks associated with the samples containing Ag_2O (s4 and s6) and the functional groups involved in the oxidation process, are examined in the 400–4000 cm^{-1} range (Fig. 13b). In addition, changes in bimetallic samples may be caused by shifts in interference between Au and Ag oscillation. Following, it can be seen that with increased

concentration of silver, remarkable changes are seen in bimetallic structures (Fig. 13c) [95].

In the FT-IR spectrum (Fig. 13a), the broad peak between 3200 and 3600 cm^{-1} belongs to the stretching vibration of O–H molecules. There are strong interactions between noble metal NPs and O–H molecules. The absorption band at 2480 cm^{-1} is observed only in the s4 which is oxidized and the concentration of silver is twice that of gold. Molecules of CO_2 in the ambient air are observed in the vicinity of 2080–1640 cm^{-1} associated with C=C bending vibration mode, which is attributed to carbon dioxide present in the atmosphere. The absorption band at 1240 cm^{-1} is caused by the hydrogen and non-hydrogen bonds of C–O stretching in a liquid medium. The peak at 1010 cm^{-1} is attributed to the stretching vibrations of C–O–H and C–O bonds [96]. The IR absorption bands at 2360 cm^{-1} in the spectrum correspond to the O–H stretching vibration [97]. The peaks of Au/Ag BNPs, illustrate the vibration properties of NPs at 719 cm^{-1} . These specified functional groups could have been involved in reducing of the metal ions and donating electrons to the stability of NPs and helping to prevent their agglomeration. These compounds play a key role in the reduction, surface functionalization, and synthesis of Au/Ag BNPs [98–100] (Table 7).

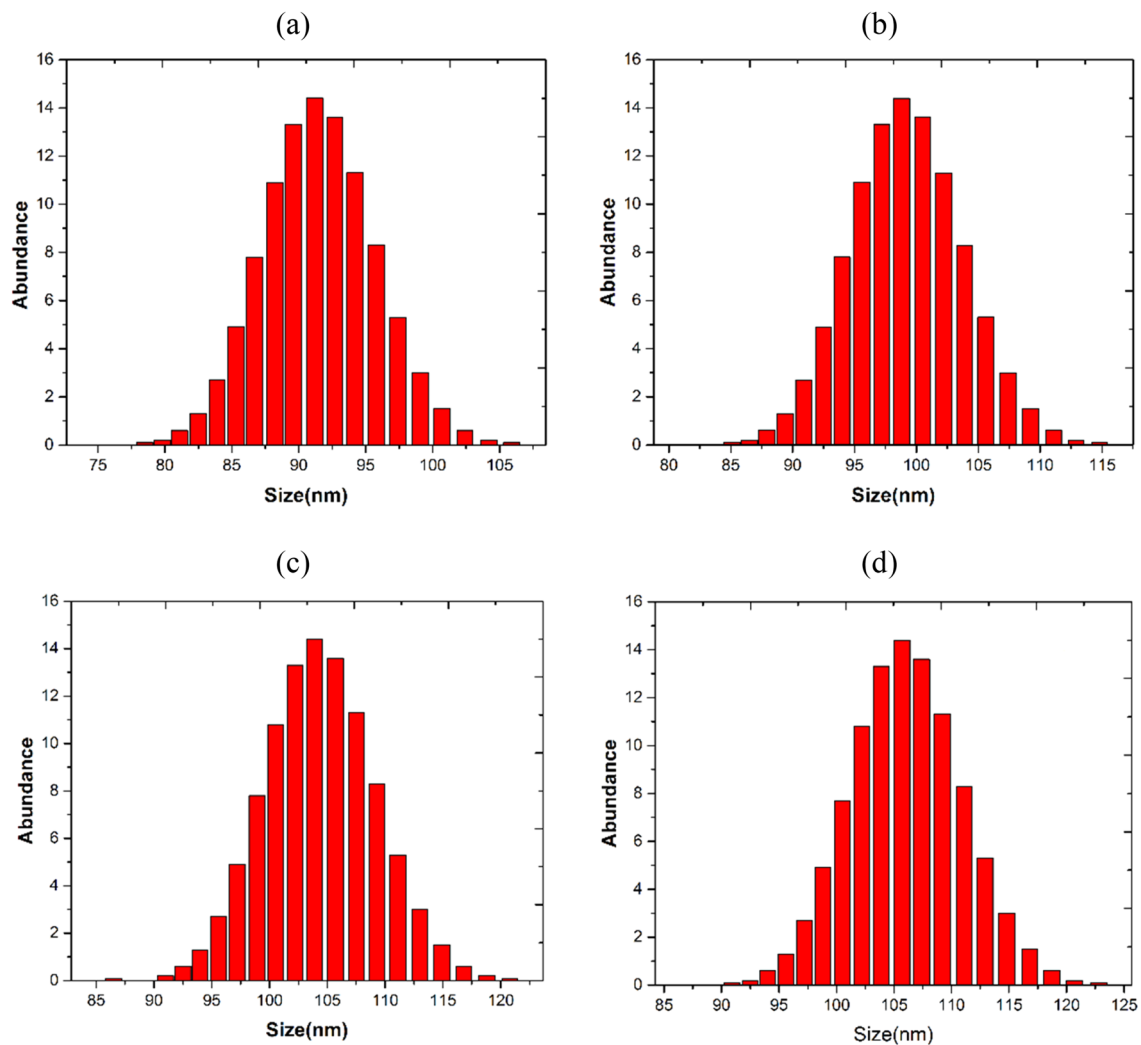


Fig. 12 DLS plots of Au/Ag BNPs produced by laser ablation technique

Table 5 The size of BNPs obtained from XRD, TEM and DLS analysis

| Sample (#) | Size (nm) | | |
|------------|-----------|-----|-------|
| | XRD | TEM | DLS |
| s1 | 16 | 9 | 92.4 |
| s2 | 22 | 18 | 100.2 |
| s3 | 28 | 23 | 105.4 |
| s4 | 32 | 34 | 107.1 |

These absorption peaks agree with the study of Weng and co-workers investigating functionalized BNPs by using specific proteins [97]. Moshfegh and colleagues observed the same absorption peak for gold, silver, and Au/Ag BNPs

in biological synthesis by amylase [101]. According to previous studies, the metal–oxygen stretching molecules were observed at 500–600 cm^{-1} [102]. Vinay and colleagues reported the band at 520 cm^{-1} that confirms the formation of Ag_2O [84]. Workneh Shume and co-workers observed the weak band at 588.29 cm^{-1} attributed to the Ag–O vibration [103]. In this study, the strength band is identified in the vicinity of 723–690 cm^{-1} assigned to the Ag–O vibration including water and Ag_2O (Fig. 13b and c). The displacement of FT-IR spectral peaks relative to the O–H molecules is directly dependent on the Ag^+ redox reaction and the formation of Au/Ag BNPs [97]. Figure 13c seen sharp peak belonging to silver NPs are more intense than those from

Table 6 Hydrodynamic radius of Au/Ag BNPs and monometallic gold and silver NPs

| Sample (#) | s1 | s2 | s3 | s4 | s5 | s6 |
|--------------------------|------|-------|-------|-------|------|------|
| Hydrodynamic radius (nm) | 92.4 | 100.2 | 105.4 | 107.1 | 78.7 | 90.6 |

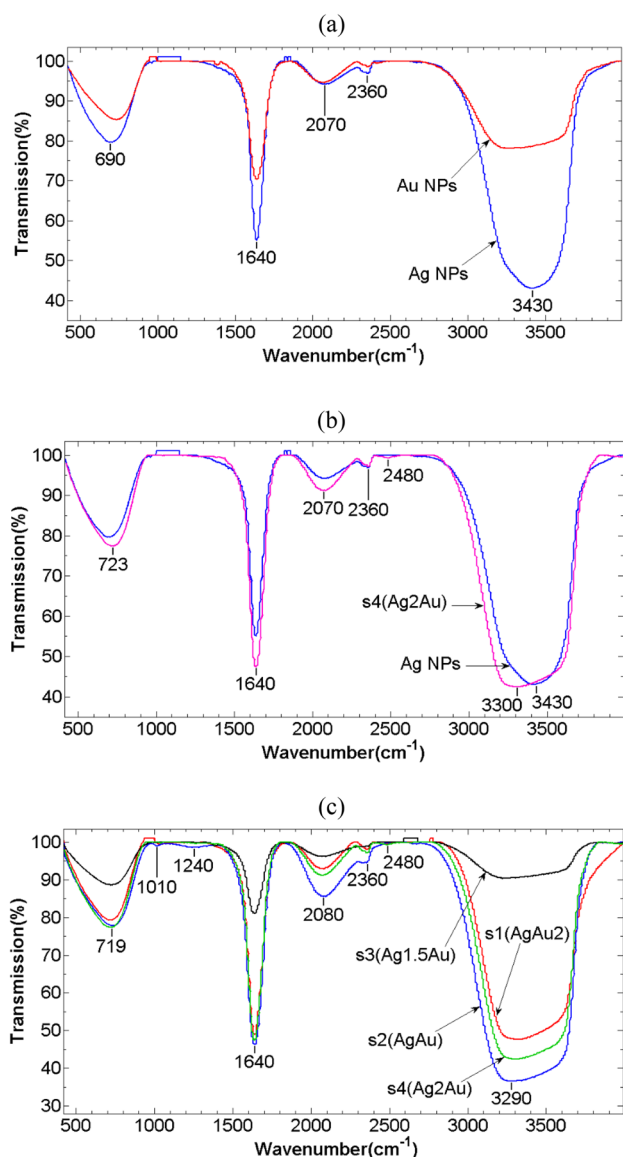


Fig. 13 Fourier transform infrared (FTIR) spectrum Au/Ag BNPs **a**, synthesized s4 and bulk AgNPs **b** and Au and AgNPs **c** with second harmonic irradiation

AuNPs. The intense peak of the AgNPs shows a larger effect of capping silver compared to AuNPs [98]. Also, the decrease in the height of the OH stretch peaks in s3 compared with other samples can be attributed to the interactions between Au/Ag BNPs and OH groups of H₂O molecules and the reduction of the capping effect on silver due to the sudden increase in the Ag concentration ratio [104].

Table 7 Chemical bonds in different wavelength for synthesized monometallic gold and silver NPs and Au/Ag BNPs

| Chemical bonds | O–H | O–H | C=C | C=O | C–O | C–O–H C–O | C–H |
|--------------------------------|------|------|------|------|------|--------------|-----|
| Wavelength (cm ⁻¹) | 3290 | 2360 | 2080 | 1640 | 1240 | 1010 | 719 |

4.5 Photoluminescence (PL) spectrum

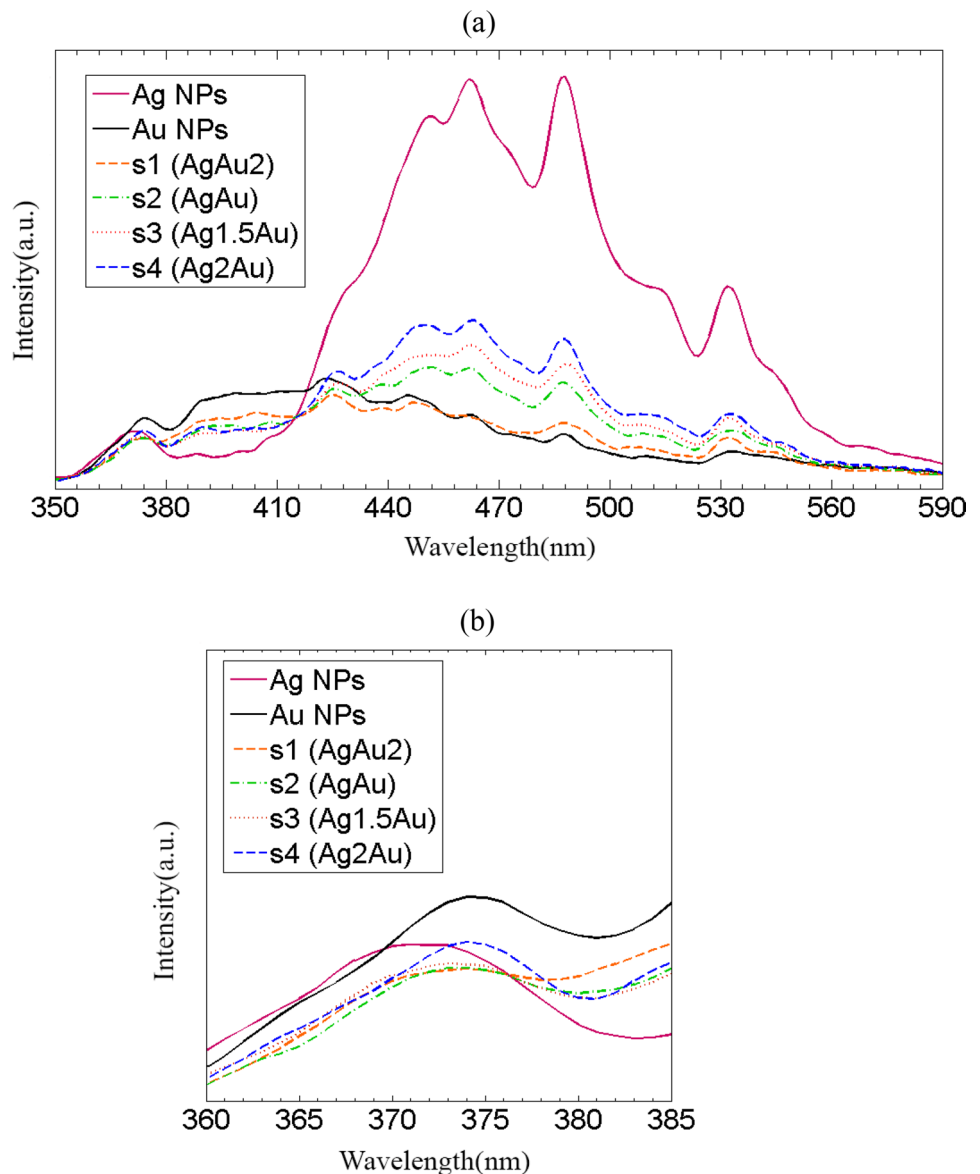
This work investigates the photoluminescence (PL) properties of Au/Ag BNPs in DIW with different volumetric ratios of AgNPs. PL measurement is regulated at room temperature with an excitation wavelength of 300 nm and the form of the PL peak is independent of the excitation wavelength. If only the volumetric fractal of silver NPs and the interaction between gold and silver NPs is increased, the intensity of PL peaks is enhanced. The redshift is identified by the interface interaction between gold and silver NPs, which is interfered with in terms of the LSPR of the Au/Ag BNPs because of the change in the size and the shift of the photoluminescence spectrum. Moreover, the broad and intense peak for Au/Ag BNPs with various crystalline sizes is observed. In the ultra-violet area, the peak of AuNPs is more significant than in other samples due to the plasmonic resonance effect. Since the plasmon resonance spectra of gold NPs strongly depend on the particle sizes, the luminescent enhancement is also dependent on the particle sizes. Moreover, gold NPs show the local electric field due to the LSPR effect. While the laser beam irradiates on the surface of the gold target, the LSPR of the gold NPs is excited and the electromagnetic field around the NPs is increased. As a result, photoluminescence absorption also grows.

The PL study is an effective technique for characterizing charge carrier separation efficiency in p-type semiconductors (in s4 and s6). It is seen that their PL intensity in the visible region is changed. In the visible region, the most substantial peak belongs to AgNPs which occur because of electron–hole recombination [33]. In s1–s3 the ratio concentration of AgNPs is below the fraction ratio threshold, and Ag₂O is not detected. In this case, charges from the surface of gold atoms are transferred without any obstacle to silver NPs and lead to decreasing the recombination between oxygen molecules and AgNPs in the ablation medium [105, 106]. By over the concentration threshold, Ag₂O in s4 is produced that confirmed by the XRD technique. The silver NPs, especially in s4 and s6 with exposure to a liquid medium, is reduced and turned into a semiconductor. Generally, in s4 and s6 during the ablation process, due to interaction between AgNPs and oxygen molecules, with the lowest probability Ag⁺ are placed in substitutional Au⁺ or interstitial positions and create more minor lattice defects. This leads to less electron–hole recombination and increasing visible emissions [107, 108].

Figure 14 illustrates several PL absorptions of Au/Ag BNPs in the range of 360–560 nm that are elicited by 532 nm laser and show efficient shifts because of the solid LSPR coupling and interband transition. There are mainly eight peaks: the first is located between 365 and 380 nm; the second is around 420–430 nm; the third is in the vicinity of 443–455 nm; the fourth is around 457–473 nm; the fifth is in the range of 480–495 nm; the sixth is between 503 and 520 nm; the seventh is nearby 525–540 nm; and the last is between 543 and 554 nm. Whether or not the height of the PL peak becomes stronger and more intense, the crystallite size of Au/Ag BNPs becomes bigger. In addition, agglomeration and adhesion lead to more interface in the bimetallic systems, resulting in increased PL absorption of samples. Several peaks in the photoluminescence spectra of Au/Ag BNPs are observed in the

range of 365–380 nm (~ 3.3 eV), which present a red-shift and noticeable increase from s1 to s4, respectively. In other work, broad blue luminescence peaks around 360 nm (~ 3.5 eV) are reported for gold and silver NPs [47]. There are other peaks in the photoluminescence spectra of Au/Ag BNPs in the ranges of 415–435 nm, which are redshifted and their height of them may be influenced by the enhancement of interactions between Au/Ag BNPs due to the increase of the volumetric ratio of AgNPs and emission intensity. Similar research about synthesizing gold and silver NPs recognized the same peaks in the vicinity of 425 nm (~ 2.91 eV) for gold NPs and 420 nm (~ 2.95 eV) for silver NPs, respectively [47]. Recently, Zakaria et al. reported the same emission (above the energy of the AgNPs bandgap) around 2.95 eV (420 nm), which shows a wide peak for silver nano-flowers [23]. The bands

Fig. 14 Photoluminescence Spectrum of the Au, AgNPs and Au/Ag BNPs **a** Magnified wavelength range of 360 nm to 385 nm **b**



corresponding to 440–470 nm transition are identified in the spectrums of the samples containing the Au/Ag BNPs. The peak of s_1 is very close to the photoluminescence band of s_6 . In other work, LSPR excitation for individual silver NPs is found around 422–455 nm (~ 2.93 – 2.72 eV) which is redshifted [47]. In some research about PANI-nanowire-Au nano-composites, a peak appeared near 460 nm (~ 2.69 eV) [105]. The intense and strong peaks are identified in a range of 480–490 nm (~ 2.55 eV) and note that the plasmon peaks illustrate blueshift with increasing crystallite size. The recognized blueshift in the plasmon absorption peak may be attributed to the quantum size effects in the silver NPs. A growth trend in the crystalline size can be observed with increasing the volumetric ratio of silver NPs. The optical coupling between this core–shell structure shows a blueshift behavior, when the AuNPs electromagnetic field interacts with AgNPs and the dielectric is changed. Observing soft peaks from 505 to 520 nm (~ 2.45 – 2.38 eV), present that if the grain size of BNPs is decreased, the pretend of optical coupling between Au/Ag BNPs and PL peak are disappeared [66]. In research about gold NPs on porous silicon, is observed a weak and broad peak is nearby 515 nm (~ 2.4 eV) [106]. Other PL spectrum reveals during 527–540 nm (~ 2.35 – 2.29 eV) which is reported in another work by R. Zakaria et al. in the vicinity of 535 nm (~ 2.31 eV). The last weak peak that is observed in the region of 543–554 nm (~ 2.28 – 2.23 eV), also is recorded for gold and silver nano-flowers during 550 nm (~ 2.25 eV) [23].

5 Summary and conclusion

In the present study, we have successfully used a laser ablation technique for the preparation of Au/Ag BNPs with alloy and core–shell structures. It has been observed that the volumetric concentration of the gold and silver NPs is affected by the optical properties of the Au/Ag BNPs. All applied analyses agree with the reported results for grain size, morphology, chemical composition, functional groups, and optical properties. The study revealed that the silver concentration and laser wavelength in the synthesis of Au/Ag BNPs, cause increased of crystalline structure and grain size, and thus the reduction Ag_2O .

One of the goals of this research is to synthesize plasmonic Au/Ag BNPs and increase the stability of silver in the compounds. The synthetic method used in this research controls the toxicity and reactivity of silver as NPs with high antimicrobial capacity. The cytotoxicity of silver NPs can be described on the basis of oxidative damage by the generation of free radicals. The non-toxic and ecological character of Au/Ag BNPs can be attributed to the molecules responsible for reduction and stabilization.

Explain the mechanism of the anti-microbial action of silver, contributed to the large surface area of AgNPs and the positively charged Ag^+ around the BNPs. Increasing the accumulation of Ag^+ in the s_1 – s_3 , when the BNPs are not oxidized and the toxic compound is not created, is the best option for the microbicide in food packaging. In addition, it is shown that all samples illustrate significant electromagnetic fields from dipole plasmon resonances in visible ranges. Since there are no quadrupole plasmonic resonances in the ultraviolet region for s_4 – s_6 , minimal improvement is recorded. This conclusion shows that even beyond a silver concentration threshold, at different wavelengths the amount of dispersion and the plasmonic behavior of metal NPs are different.

These results denote current bimetallic samples and may be applied to nano-biosensors to detect different kinds of proteins. In addition, as Au/Ag BNPs containing silver are the most important in the food packaging industry, the next step would be to study the antibacterial responses of Au/Ag BNPs. By introducing the synthesized bimetallic system into the polymer matrix and forming of the nanocomposite, it is possible to supply the basic nanomaterials necessary for packaging.

Acknowledgements The authors are thankful to the Science and Research Branch of Islamic Azad University (SRBIAU) and especially the Laser laboratory of Plasma Physics Research Center (PPRC) for providing all the necessary facilities. Likewise, we acknowledge the TEM operator Mr. Hosseinpour of Khajeh Nasir University (KNU) for his significant advice. In addition, we are extremely grateful to our research would not have been possible without the nurturing of Elham Mohebi.

Author contributions The authors confirm contribution to the paper as follows: AHS devised the project, AHS presented the main conceptual ideas, AHS encouraged SAA to investigate a specific aspect of Au/Ag BNPs and supervised the findings of this work, DD designed the experimental framework, DD and SAA contributed to laser preparation, AHS and DD verified the analytical methods, SAA worked out almost all of the experiment, EM fabricated the samples, SAA analyzed all of the spectra, SAA wrote the manuscript with support from AHS and DD, all authors contributed to the final version of the manuscript.

Funding The Authors declare that no funds, grants, or other support were received during the preparation of this manuscript.

Declarations

Conflict of interest All authors declare that they have no conflicts of interest.

Open Access This article is licensed under a Creative Commons Attribution 4.0 International License, which permits use, sharing, adaptation, distribution and reproduction in any medium or format, as long as you give appropriate credit to the original author(s) and the source, provide a link to the Creative Commons licence, and indicate if changes were made. The images or other third party material in this article are included in the article's Creative Commons licence, unless

indicated otherwise in a credit line to the material. If material is not included in the article's Creative Commons licence and your intended use is not permitted by statutory regulation or exceeds the permitted use, you will need to obtain permission directly from the copyright holder. To view a copy of this licence, visit <http://creativecommons.org/licenses/by/4.0/>.

References

1. Sharma G, Kumar D, Kumar A, Al-Muhtaseb AH, Pathania D, Naushad M, Mola GT (2017) Revolution from monometallic to trimetallic nanoparticle composites, various synthesis methods and their applications: A review. *Mater Sci Eng C* 71:1216–1230. <https://doi.org/10.1016/j.msec.2016.11.002>
2. Ferreira E, Kharisov B, Vázquez A, Méndez EA, Severiano-Carrillo I, Trejo-Durán M (2019) Tuning the nonlinear optical properties of Au@Ag bimetallic nanoparticles. *J Mol Liquids* 298:112057. <https://doi.org/10.1016/j.molliq.2019.112057>
3. Jagannath G, Eraiah B, NagaKrishnakanth K, Venugopal Rao S (2018) Linear and nonlinear optical properties of gold nanoparticles doped borate glasse. *J Non-Cryst Solids* 482:160–169. <https://doi.org/10.1016/j.jnoncrysol.2017.12.036>
4. Mostafa AM, Mwafy EA, Awwad NS, Ibrahim HA (2021) Au@Ag core/shell nanoparticles prepared by laser-assisted method for optical limiting applications. *J Mater Sci Mater Electron* 32:14728–14739. <https://doi.org/10.1007/s10854-021-06028-9>
5. Jagannath G, Eraiah B, Jayanthi K, Keshri SR, Som S, Vinita G, Pramod AG, Krishnakanth KN, Devarjulu G, Balaji S, Rao SV, Annapurna K, Das S, Allu AR (2020) Influence of gold nanoparticles on the nonlinear optical and photoluminescence properties of Eu₂O₃ doped alkali borate glasses. *Phys Chem* 22:2019–2032. <https://doi.org/10.1039/C9CP05783H>
6. Dsouza A, Shilpa MP, Gurumurthy SC, Nagaraja BS, Mundinamani S, Ramam K, Gedda M, Murari MS (2021) CuAg and AuAg bimetallic nanoparticles for catalytic and heat transfer applications. *Clean Technol Environ Policy* 23:2145–2155. <https://doi.org/10.1007/s10098-021-02120-0>
7. Çiplak Z, Gökalp C, Getiren B, Yıldız A, Yıldız N (2018) Catalytic performance of Ag, Au and Ag–Au nanoparticles synthesized by lichen extract. *Green Process Synth* 7:433–440. <https://doi.org/10.1515/gps-2017-0074>
8. Falahati M, Attar F, Sharifi M, Saboury AA, Salihi A, Aziz FM, El-Sayed MA (2020) Gold nanomaterials as key suppliers in biological and chemical sensing, catalysis, and medicine. *Biochim Biophys Acta (BBA) General Subjects* 1864(1):129435. <https://doi.org/10.1016/j.bbagen.2019.129435>
9. Iravani S, Korbekandi H, Mirmohammadi SV, Zolfaghari B (2014) Synthesis of silver nanoparticles: chemical, physical and biological Methods. *J Res Pharm Sci* 9:385–406
10. Biswas R, Das SK, Bhaduri SN, Bhaumik A, Biswas P (2020) AgNPs immobilized over functionalized 2D Hexagonal SBA-15 for Catalytic C–H oxidation of hydrocarbons with molecular oxygen under solvent-free conditions. *ACS Sustain Chem Eng* 8:5856–5867. <https://doi.org/10.1021/acssuschemeng.9b07409>
11. Vinay SP, Udayabhanu NG, Chandrappa CP, Chandrasekhar N (2019) Enhanced photocatalysis, photoluminescence, and anti-bacterial activities of nanosize Ag: green synthesized via *Rauvolfia tetraphylla* (devil pepper). *SN Appl Sci* 1:477. <https://doi.org/10.1007/s42452-019-0437-0>
12. Monga A, Pal B (2015) Improved catalytic activity and surface electro-kinetics of bimetallic Au–Ag core–shell nanocomposites. *New J Chem* 39:304–313. <https://doi.org/10.1039/C4NJ01419G>
13. Karaduman I, Er E, Çelikkan H, Erk N, Acar S (2017) Room-temperature ammonia gas sensor based on reduced graphene oxide nanocomposites decorated by Ag, Au and Pt nanoparticles. *J Alloys Compd* 722:569–578. <https://doi.org/10.1016/j.jallcom.2017.06.152>
14. Bitton O, Gutman DB, Berkovits R, Frydman A (2017) Multiple periodicity in a nanoparticle-based single-electron transistor. *Nat Commun* 8:402. <https://doi.org/10.1038/s41467-017-00442-6>
15. Arora N, Mehta A, Mishra A, Basu S (2018) 4-Nitrophenol reduction catalysed by Au–Ag bimetallic nanoparticles supported on LDH: homogeneous vs. heterogeneous catalysis. *Appl Clay Sci* 151:1–9. <https://doi.org/10.1016/j.clay.2017.10.015>
16. Bu Y, Lee SW (2015) The characteristic Ag_{core}Au_{shell} nanoparticles as SERS substrates in detecting dopamine molecules at various pH ranges. *Int J Nanomed* 10:47–54
17. Crespo J, Falqui A, García-Barrasa J, López-de-Luzuriaga JM, Monge M, Olmos ME, Soulantica K (2014) Synthesis and plasmonic properties of monodisperse Au–Ag alloy nanoparticles of different compositions from a single-source organometallic precursor. *J Mater Chem C* 2(16):2975–2984. <https://doi.org/10.1039/c3tc32577f>
18. Orendorff CJ, Sau TK, Murphy CJ (2006) Shape-dependent Plasmon-resonant gold nanoparticles. *Small* 2(5):636–639. <https://doi.org/10.1002/sml.200500299>
19. Fuchs R (1987) Multipolar response of small metallic spheres: nonlocal theory. *Phys Rev B* 35:3722–3727. <https://doi.org/10.1103/physrevb.35.3722>
20. Kolwas K, Derkachova A (2020) Impact of the interband transitions in gold and silver on the dynamics of propagating and localized surface Plasmons. *Nanomaterials* 10:1411. <https://doi.org/10.3390/nano10071411>
21. Mahmud S, Sharmin Satter S, Singh AK, Rahman MM, Mollah MYA, Hasan Susan MdAB (2019) Tailored engineering of bimetallic plasmonic Au@Ag Core@Shell nanoparticles. *ACS Omega* 4:18061–18075. <https://doi.org/10.1021/acsomega.9b01897>
22. Hutter E, Fendler JH (2004) Exploitation of localized surface Plasmon resonance. *Adv Mater* 16:1685–1706. <https://doi.org/10.1002/adma.200400271>
23. Zakaria R, Hamdan KS, Noh SMC, Supangat A, Sookhakian M (2015) Surface Plasmon resonance and photoluminescence studies of Au and Ag micro-flowers. *Opt Mater Exp* 5:943–950. <https://doi.org/10.1364/OME.5.000943>
24. Zhang D, Li Z, Sugioka K (2021) Laser ablation in liquids for nanomaterial synthesis: diversities of targets and liquids. *J Phys Photonics* 3:042002. <https://doi.org/10.1088/2515-7647/ac0bfd>
25. Mahfouz R, Cadete Santos Aires FJ, Brenier A, Ehret E, Roumié M, Nsouli B, Bertolini JC (2010) Elaboration and characterization of bimetallic nanoparticles obtained by laser ablation of Ni₇₅Pd₂₅ and Au₇₅Ag₂₅ targets in water. *J Nanoparticle Res* 12:3123–3136. <https://doi.org/10.1007/s11051-010-9949-7>
26. Amendola V, Meneghetti M (2013) What controls the composition and the structure of nanomaterials generated by laser ablation in liquid solution. *Phys Chem Chem Phys* 15:3027–3046. <https://doi.org/10.1039/c2cp42895d>
27. Liu P, Cui H, Wang CX, Yang GW (2010) From nanocrystal synthesis to functional nanostructure fabrication: laser ablation in liquid. *Phys Chem Chem Phys* 12:3942–3952. <https://doi.org/10.1039/b918759f>
28. Kaçuş H, Metin Ö, Sevim M, Biber M, Baltakesmez A, Aydoğan Ş (2021) A comparative study on the effect of monodisperse Au and Ag nanoparticles on the performance of organic

- photovoltaic devices. *Opt Mater* 116:111082. <https://doi.org/10.1016/j.optmat.2021.111082>
29. McGilvray KL, Fasciani C, Alejo CJB, Narbonne RS, Scaiano JC (2012) Photochemical strategies for the seed-mediated growth of gold and gold-silver nanoparticles. *Langmuir* 28:16148–16155. <https://doi.org/10.1021/la302814v>
 30. Pei F, Wu S, Wang G, Xu M, Wang SY, Chen LY (2009) Electronic and optical properties of noble metal oxides (M = Cu, Ag and Au): first-principles study. *J Korean Phys Soc* 55:1243–1249. <https://doi.org/10.3938/jkps.55.1243>
 31. Zhang Q, Xie J, Lee JY, Zhang J, Boothroyd C (2008) Synthesis of Ag@AgAu metal core/alloy shell bimetallic nanoparticles with Tunable Shell compositions by a galvanic replacement reaction. *Small* 4:1067–1071. <https://doi.org/10.1002/sml.200701196>
 32. Berahim N, Basirun WJ, Leo BF, Johan MR (2018) Synthesis of bimetallic gold-silver (Au–Ag) nanoparticles for the catalytic reduction of 4-Nitrophenol to 4-Aminophenol. *Catalysts* 18:412. <https://doi.org/10.3390/catal18100412>
 33. Kumar N, Alam F, Dutta V (2014) Deposition of Ag and Au–Ag alloy nanoparticle films by spray pyrolysis technique with tuned plasmonic properties. *J Alloys Compd* 585:312–317. <https://doi.org/10.1016/j.jallcom.2013.09.145>
 34. Duan S, Wang R (2013) Bimetallic nanostructures with magnetic and noble metals and their physicochemical applications. *Mater Int* 23:113–126. <https://doi.org/10.1016/j.pnsc.2013.02.001>
 35. Sheny DS, Mathew J, Philip D (2011) Phytosynthesis of Au, Ag and Au–Ag bimetallic nanoparticles using aqueous extract and dried leaf of *Anacardium occidentale*. *Spectrochimica Acta Part A* 79:254–262. <https://doi.org/10.1016/j.saa.2011.02.051>
 36. AbdelHamid AA, Al-Ghobashy M, Fawzy M, Mohamed M, Abdel-Mottaleb MMSA (2013) Phytosynthesis of Au, Ag and Au–Ag bimetallic nanoparticles using aqueous extract of sago pondweed (*Potamogeton pectinatus* L.). *ACS Sustain Chem Eng* 1:1520–1529. <https://doi.org/10.1021/sc4000972>
 37. Sharma C, Ansari AMS, Satsangee SP, Srivastava MM (2020) Single-step green route synthesis of Au/Ag bimetallic nanoparticles using clove buds extract: enhancement in antioxidant bio-efficacy and catalytic activity. *Mater Sci Eng C* 116:111153. <https://doi.org/10.1016/j.msec.2020.111153>
 38. Estakhri S, Darabi E, Adergani BA, Elahi SM (2022) Photoluminescence study of Au–Ag bimetallic nanoparticles supported on mesoporous silica SBA-15. *J Theor Appl Phys* 16:1–6. <https://doi.org/10.30495/jtap.162229>
 39. Kohut A, Péter Villy L, Kéri A, Béltéki Á, Megyeri D, Hopp B, Galbács G, Geretovszky Z (2021) Full range tuning of the composition of Au/Ag binary nanoparticles by spark discharge generation. *Sci Rep* 11:5117. <https://doi.org/10.1038/s41598-021-84392-6>
 40. Nikov RG, Nedyalkov NN, Atanasov PA, Karashanova DB (2018) Synthesis of bimetallic nanostructures by nanosecond laser ablation of multicomponent thin films in water. *J Phys* 992:012046. <https://doi.org/10.1088/1742-6596/992/1/012046>
 41. Mamonova DV, Vasileva AA, Petrov YV, Koroleva AV, Danilov DV, Kolesnikov IE, Bikbaeva GI, Bachmann J, Manshina AA (2022) Single step laser-induced deposition of plasmonic Au, Ag, Pt Mono- Bi- and Tri-Metallic nanoparticles. *Nanomaterials* 12:146. <https://doi.org/10.3390/nano12010146>
 42. Verma S, Rao BT, Detty AP, Ganesan V, Phase DM, Rai SK, Bose A, Joshi SC, Kukreja LM (2015) Surface plasmon resonances of Ag–Au alloy nanoparticle films grown by sequential pulsed laser deposition at different compositions and temperatures. *J Appl Phys* 117:133105. <https://doi.org/10.1063/1.4916750>
 43. Tarasenko NV, Butsen AV (2010) Laser synthesis and modification of composite nanoparticles in liquids. *Quantum Electron* 40:986–1003. <https://doi.org/10.1070/QE2010v040n11ABEH014446>
 44. Kuladeep R, Jyothi L, Shadak Alee K, Deepak KLN, Narayana Rao D (2012) Laser-assisted synthesis of Au–Ag alloy nanoparticles with tunable surface plasmon resonance frequency. *Opt Mater Exp* 2:161–172. <https://doi.org/10.1364/OME.2.000161>
 45. Sebastian S, Linslal CL, Vallbhan CPG, Nampoori VPN, Radhakrishnan P, Kailasnath M (2015) Formation of Au–Ag nanoalloy through Au core/Ag shell intermediate phase by laser ablation. *Chem Phys Lett* 628:25–29. <https://doi.org/10.1016/j.cplett.2015.03.034>
 46. Alarcón LE, Granados EV, Sanchez DV, Mejía OO, Poniatowski EH, Castañeda AA, Solís-Casados DA (2014) Bismuth and gold nanoparticles prepared by laser ablation in aqueous solutions. *Adv Mater Res* 976:196–201. <https://doi.org/10.4028/www.scientific.net/AMR.976.196>
 47. Solati E, Dorrnian D (2015) Comparison between silver and gold nanoparticles prepared by pulsed laser ablation in distilled water. *J Clust Sci* 26:727–742. <https://doi.org/10.1007/s10876-014-0732-2>
 48. Olea-Mejía O, Fernández-Mondragón M, Rodríguez-de la Concha G, Camacho-López M (2015) SERS-active Ag, Au and Ag–Au alloy nanoparticles obtained by laser ablation in liquids for sensing methylene blue. *Appl Surf Sci* 348:66–70. <https://doi.org/10.1016/j.apsusc.2015.01.075>
 49. Vinod M, Gopchandran KG (2015) Ag@Au core-shell nanoparticles synthesized by pulsed laser ablation in water: effect of plasmon coupling and their SERS performance. *Spectrochim Acta Part A Mol Biomol Spectrosc* 149:913–919. <https://doi.org/10.1016/j.saa.2015.05.004>
 50. Vinod M, Biju V, Gopchandran KG (2016) Studies on plasmon characteristics and the local density of states of Au and Ag based nanoparticles. *Superlattices Microstruct* 89:369–377. <https://doi.org/10.1016/j.spmi.2015.11.035>
 51. Al-Azawi MA, Bidin N, Bououdina M, Mohammad SM (2016) Preparation of gold and gold-silver alloy nanoparticles for enhancement of plasmonic dye-sensitized solar cells performance. *Sol Energy* 126:93–104. <https://doi.org/10.1016/j.solener.2015.12.043>
 52. Loza K, Heggen M, Epple M (2020) Synthesis, structure, properties, and applications of bimetallic nanoparticles of noble metals. *Adv Funct Mater*. <https://doi.org/10.1002/adfm.201909260>
 53. Awwad NS, Abd El-Kader MFH, Ibrahim HA, Asnag GM, Morsi MA (2021) Green synthesis of different ratios from bimetallic gold: silver nanoparticles core@shell via laser ablation scattered in Chitosan-PVA matrix and its electrical conductivity behavior. *Compos Commun* 24:100678. <https://doi.org/10.1016/j.coco.2021.100678>
 54. Abed MA, Mutlak FAH, Ahmed AF, Nayef UM, Abdulridha SK (2021) Synthesis of Ag/Au (core/shell) nanoparticles by laser ablation in liquid and study of their toxicity on blood human components. *J Phys Conf Series* 1795:012013. <https://doi.org/10.1088/1742-6596/1795/1/012013>
 55. Jiang Z, Li L, Huang H, He W, Ming W (2022) Progress in laser ablation and biological synthesis processes: “Top-Down” and “Bottom-Up” approaches for the green synthesis of Au/Ag nanoparticles. *Int J Mol Sci* 23:14658. <https://doi.org/10.3390/ijms232314658>
 56. Link S, El-Sayed MA (1999) Size and temperature dependence of the plasmon absorption of colloidal gold nanoparticles. *J Phys Chem B* 103:4212–4217. <https://doi.org/10.1021/jp984796o>

57. Ganjali M, Ganjali M, Khoby S, Meshkot MA (2011) Synthesis of Au–Cu nano-alloy from monometallic colloids by simultaneous pulsed laser targeting and stirring. *Nano-Micro Lett* 3:256–263. <https://doi.org/10.3786/nml.v3i4.p256-263>
58. Dolgaev SI, Simakin AV, Voronov VV, Shafeev GA, Bozon-Verduraz F (2002) Nanoparticles produced by laser ablation of solids in liquid environment. *Appl Surf Sci* 186:546–551. [https://doi.org/10.1016/S0169-4332\(01\)00634-1](https://doi.org/10.1016/S0169-4332(01)00634-1)
59. Derkachova A, Kolwas K, Demchenko I (2016) Dielectric function for gold in plasmonics applications: size dependence of plasmon resonance frequencies and damping rates for nanospheres. *Plasmonics* 11:941–951. <https://doi.org/10.1007/s11468-015-0128-7>
60. Kumari MM, Jacob J, Philip D (2015) Green synthesis and applications of Au–Ag bimetallic nanoparticles. *Spectrochim Acta Part A Mol Biomol Spectrosc* 137:185–192. <https://doi.org/10.1016/j.saa.2014.08.079>
61. Csapó E, Oszkó A, Varga E, Juhász Á, Buzás N, Kőrösi L, Dékány I (2012) Synthesis and characterization of Ag/Au alloy and core (Ag)–shell (Au) nanoparticles. *Colloids Surf A Physicochem Eng Aspects* 415:281–287. <https://doi.org/10.1016/j.colsurfa.2012.09.005>
62. Godipurge SS, Yallappa S, Biradar NJ, Biradar JS, Dhananjaya BL, Hegde G, Jagadish K, Hegd G (2016) A facile and green strategy for the synthesis of Au, Ag and Au–Ag alloy nanoparticles using aerial parts of *R. hypocrateriformis* extract and their biological evaluation. *Enzyme Microb Technol* 95:174–184. <https://doi.org/10.1016/j.enzmictec.2016.08.006>
63. Westsson E, Koper GJM (2014) How to determine the core–shell nature in bimetallic catalyst particles. *Catalysts* 4:375–396. <https://doi.org/10.3390/catal4040375>
64. Trotter KD, Owojaiye O, Meredith SP, Keating PE, Spicer MD, Reglinski J, Spickett CM (2019) The interaction of silver (II) complexes with biological macromolecules and antioxidants. *Biomaterials* 32:627–640. <https://doi.org/10.1007/s10534-019-00198-0>
65. Nudelman R, Gavrieli S, Bychenko D, Barzilay M, Gulakhmedova T, Gazit E, Richter S (2021) Bio-assisted synthesis of bimetallic nanoparticles featuring antibacterial and photothermal properties for the removal of biofilms. *J Nanobiotechnol* 19:452. <https://doi.org/10.1186/s12951-021-01183-x>
66. Zhang T, Lu G, Shen H, Shi K, Jiang Y, Xu D, Gong Q (2014) Photoluminescence of a single complex plasmonic nanoparticle. *Sci Rep* 4:3867. <https://doi.org/10.1038/srep03867>
67. Wang L, Wang X, Luo J, Wanjala BN, Wang C, Chernova NA, Engelhard MH, Liu Y, Bae IT, Zhong CJ (2010) Core–shell-structured magnetic ternary nanocubes. *J Am Chem Soc* 132:17686–17689. <https://doi.org/10.1021/ja1091084>
68. Tsuji M, Hikino S, Tanabe R, Yamaguchi D (2010) Synthesis of Ag@Cu core-shell nanoparticles in high yield using a polyol method. *Chem Lett* 39:334336. <https://doi.org/10.1246/cl.2010.334>
69. Pyne S, Sarkar P, Basu S, Prasad Sahoo G, Bhui DK, Bar H, Misra A (2011) Synthesis and photo physical properties of Au @ Ag (core @ shell) nanoparticles disperse in poly vinyl alcohol matrix. *J Nanopart Res* 13:1759–1767. <https://doi.org/10.1007/s11051-010-9955-9>
70. Rodríguez-González B, Burrows A, Watanabe M, Kiely CJ, Marzán LML (2005) Multishell bimetallic AuAg nanoparticles: synthesis, structure and optical properties. *J Mater Chem* 15(17):1755–1759
71. Bastús NG, Piella J, Puntès V (2016) Quantifying the sensitivity of multipolar (Dipolar, Quadrupolar, and Octapolar) surface plasmon resonances in silver nanoparticles: the effect of size, composition, and surface coating. *Langmuir* 32:290–300. <https://doi.org/10.1021/acs.langmuir.5b03859>
72. Yuan P, Ma R, Gao N, Garai M, Xu QH (2015) Plasmon coupling-enhanced two-photon photoluminescence of Au@Ag core–shell nanoparticles and applications in the nuclease assay. *Nanoscale* 7:10233–10239. <https://doi.org/10.1039/C5NR01409C>
73. Harada M, Kizaki S (2016) Formation mechanism of gold nanoparticles synthesized by Photoreduction in Aqueous ethanolic solutions of polymers using in situ quick scanning X-ray absorption fine structure and small-angle X-ray scattering. *Cryst Growth Des* 16:1200–1212. <https://doi.org/10.1021/acs.cgd.5b01168>
74. Solati E, Mashayekh M, Dorrani D (2013) Effects of laser pulse wavelength and laser fluence on the characteristics of silver nanoparticle generated by laser ablation. *Appl Phys A* 112:689–694. <https://doi.org/10.1007/s00339-013-7812-2>
75. Mandal A, Bhattachary M, Kuznetsov DV, Ghosh T, Chakraborty SD, Satpati B, Mazov V, Senapati D (2018) Decoupled in-plane dipole resonance modulated colorimetric assay-based optical ruler for ultra-trace gold (Au) detection. *Sci Rep* 8:868. <https://doi.org/10.1038/s41598-018-19148-w>
76. Romero I, Aizpurua J, Bryant GW, García de Abajo FJ (2006) Plasmons in nearly touching metallic nanoparticles: singular response in the limit of touching dimers. *Opt Express* 14:9988–9999. <https://doi.org/10.1364/OE.14.009988>
77. Shore MS, Wang J, Johnston-Peck AC, Oldenburg AL, Tracy JB (2011) Synthesis of Au(Core)/Ag(Shell) nanoparticles and their conversion to AuAg alloy nanoparticles. *Small* 7:230–234. <https://doi.org/10.1002/sml.201001138>
78. Samal AK, Polavarapu L, Rodal-Cedeira S, Liz-Marzan LM, Perez-Juste J, Pastoriza-Santos I (2013) Size tunable Au@Ag core–shell nanoparticles: synthesis and surface-enhanced raman scattering properties. *Langmuir* 29(48):15076–15082. <https://doi.org/10.1021/la403707j>
79. Mallin MP, Murphy CJ (2002) Solution-phase synthesis of Sub-10 nm Au–Ag alloy nanoparticles. *Nano Lett* 2:1235–1237. <https://doi.org/10.1021/nl025774n>
80. Sharma G, Kumar A, Sharma S, Naushad M, Dwivedi RP, Alotman ZA, Mola GT (2019) Novel development of nanoparticles to bimetallic nanoparticles and their composites: a review. *J King Saud Univ Sci* 31:257–269. <https://doi.org/10.1016/j.jksus.2017.06.012>
81. Romero I, Lal S, Hafner JH, Nordlander P, Halas NJ (2008) Close encounters between two nanoshells. *Nano Lett* 8:1212–1218. <https://doi.org/10.1021/nl080271o>
82. Garcia MA (2011) Surface plasmons in metallic nanoparticles: fundamentals and applications. *J Phys D Appl Phys* 44:283001. <https://doi.org/10.1088/0022-3727/44/28/283001>
83. Desarkar HS, Kumbhakar P, Mitra AK (2013) Synthesis of silver hollow nanoparticles and observation of photoluminescence emission properties. *J Lumin* 134:1–7. <https://doi.org/10.1016/j.jlumin.2012.10.007>
84. Vinay SP, Udayabhanu NG, Chandrappa CP, Chandrasekhar N (2019) Novel Gomutra (cow urine) mediated synthesis of silver oxide nanoparticles and their enhanced photocatalytic, photoluminescence and antibacterial studies. *J Sci Adv Mater Dev* 4:392–399. <https://doi.org/10.1016/j.jsamd.2019.08.004>
85. Zhu J (2005) Theoretical study of the optical absorption properties of Au–Ag bimetallic nanospheres. *Physica E* 27:296–301. <https://doi.org/10.1016/j.physe.2004.12.006>
86. Atae-Esfahani H, Wang L, Nemoto Y, Yamauchi Y (2010) Synthesis of bimetallic Au@Pt nanoparticles with Au Core and nanostructured Pt Shell toward highly active Electrocatalysts. *Chem Mater* 22:6310–6318. <https://doi.org/10.1021/cm102074w>
87. Qu Z, Ke G, Wang Y, Liu M, Jiang T, Gao J (2013) Investigation of factors influencing the catalytic performance of CO

- oxidation over Au–Ag/SBA-15 catalyst. *Appl Surf Sci* 277:293–301. <https://doi.org/10.1016/j.apsusc.2013.04.051>
88. Kamimuraa S, Yamashita S, Abe S, Tsubota T, Ohno T (2017) Effect of core@shell (Au@Ag) nanostructure on surface plasmon-induced photocatalytic activity under visible light irradiation. *Appl Catal B* 211:11–17. <https://doi.org/10.1016/j.apcatb.2017.04.028>
89. Rick J, Tsai MC, Hwang BJ (2016) Biosensors incorporating bimetallic nanoparticles. *Nanomaterials* 6:5. <https://doi.org/10.3390/nano6010005>
90. Amikura K, Kimura T, Hamada M, Yokoyama N, Miyazaki J, Yamada Y (2008) Copper oxide particles produced by laser ablation in water. *Appl Surf Sci* 254:6976–6982. <https://doi.org/10.1016/j.apsusc.2008.05.091>
91. Zielińska-Jurek A, Reszczyńska J, Grabowska E, Zaleska A (2012) Nanoparticles Preparation Using Microemulsion Systems, Microemulsions - An Introduction to Properties and Applications. In *Tech* 12:229–250. ISBN: 978-953-51-0247-2
92. Meva FE, Ntomba AA, Ebanda Kedi PB, Tchoumbi E, Schmitz A, Schmolke L, Klopotoski M, Moll B, Kökcam-Demir Ü, Mpondo Mpondo EA, Lehman LG, Janiak C (2019) Silver and palladium nanoparticles produced using a plant extract as reducing agent, stabilized with an ionic liquid: sizing by X-ray powder diffraction and dynamic light scattering. *J Mater Res Technol* 8:1991–2000. <https://doi.org/10.1016/j.jmrt.2018.12.017>
93. Lemes MA, Rabelo D, Oliveira AED (2017) A novel method to evaluate nanofluid stability using multivariate image analysis. *Anal Methods* 9:5826–5833. <https://doi.org/10.1039/C7AY00645D>
94. Lim J, Yeap SP, Che HX, Low SC (2013) Characterization of magnetic nanoparticle by dynamic light scattering. *Nanoscale Res Lett* 8:381. <https://doi.org/10.1186/1556-276X-8-381>
95. Chen HM, Liu RS, Jang LY, Lee JF, Hu SF (2006) Characterization of core-shell type and alloy Ag/Au bimetallic clusters by using extended X-ray absorption fine structure spectroscopy. *Chem Phys Lett* 421:118–123. <https://doi.org/10.1016/j.cplett.2006.01.043>
96. Shkryl Y, Rusapetova T, Yugay Y, Egorova A, Silant'ev V, Grigoruk V, Bulgakov V (2021) Biosynthesis and cytotoxic properties of Ag, Au, and bimetallic nanoparticles synthesized using *Lithospermum erythrorhizon* callus culture extract. *Int J Mol Sci* 22(17):9305. <https://doi.org/10.3390/ijms22179305>
97. Weng Y, Li J, Ding X, Wang B, Dai S, Zhou Y, Pang R, Zhao Y, Xu H, Tian B, Hua Y (2020) Functionalized gold and silver bimetallic nanoparticles using *Deinococcus radiodurans* protein extract mediate degradation of toxic dye malachite green. *Int J Nanomed* 15:1823–1835. <https://doi.org/10.2147/IJN.S236683>
98. Elemike EE, Onwudiwe DC, Fayemi OE, Botha TL (2019) Green synthesis and electrochemistry of Ag, Au, and Ag–Au bimetallic nanoparticles using golden rod (*Solidago canadensis*) leaf extract. *Appl Phys A* 125:42. <https://doi.org/10.1007/s00339-018-2348-0>
99. Abbasi BH, Zaka M, Hashmi SS, Khan Z (2018) Biogenic synthesis of Au, Ag and Au–Ag alloy nanoparticles using *Cannabis sativa* leaf extract. *IET Nanobiotechnol* 12:277–284. <https://doi.org/10.1049/iet-nbt.2017.0169>
100. Khan M, Al-hamoud K, Liaqat Z, Shaik MR, Adil SF, Kuniyil M, Alkhatlan HZ, Al-Warthan A, Siddiqui MRH, Mondeshki M, Tremel W, Khan M, Tahir MN (2020) Synthesis of Au, Ag, and Au–Ag bimetallic nanoparticles using *Pulicaria undulata* extract and their catalytic activity for the reduction of 4-Nitrophenol. *Nanomaterials* 10:1885. <https://doi.org/10.3390/nano10091885>
101. Moshfegh M, Frootanfar H, Zare B, Shahverdi AR, Zarrini G, Faramarzi MA (2011) Biological synthesis of Au, Ag and Au–Ag bimetallic nanoparticles by α -amylase. *Dig J Nanomater Biostruct* 6:1419–1426
102. Ravichandran S, Paluri V, Kumar G, Loganathan K, Venkata BRK (2015) A novel approach for the biosynthesis of silver oxide nanoparticles using aqueous leaf extract of *Callistemon lanceolatus* (Myrtaceae) and their therapeutic potential. *J Exp Nanosci* 11:445–458. <https://doi.org/10.1080/17458080.2015.1077534>
103. Shume WM, Murthy HCA, Zereffa EA (2020) A review on synthesis and characterization of Ag_2O nanoparticles for photocatalytic applications. *J Chem*. <https://doi.org/10.1155/2020/5039479>
104. Manchala S, Nagappagari LR, Venkatakrishnan SM, Shanker V (2019) Solar-light harvesting bimetallic Ag/Au decorated graphene Plasmonic system with efficient Photoelectrochemical performance for the enhanced water reduction process. *ACS Appl Nano Mater* 2:4782–4792. <https://doi.org/10.1021/acsnano.9b00684>
105. Samanta A, Gangopadhyay R, Ghosh CK, Ray M (2017) Enhanced photoluminescence from gold nanoparticle decorated polyaniline nanowire bundles. *RSC Adv* 7:27473. <https://doi.org/10.1039/c7ra01124e>
106. Amran TST, Hashim MR, Al-Obaidi NKA, Yazid H, Adnan R (2013) Optical absorption and photoluminescence studies of gold nanoparticles deposited on porous silicon. *Nanoscale Res Lett* 8:35. <https://doi.org/10.1186/1556-276X-8-35>
107. Ziashahabi A, Prato M, Dang Z, Poursalehi R, Naseri N (2019) The effect of silver oxidation on the photocatalytic activity of Ag/ZnO hybrid plasmonic/metal-oxide nanostructures under visible light and in the dark. *Sci Rep* 9:11839. <https://doi.org/10.1038/s41598-019-48075-7>
108. Santana LA, Reséndiz LM, Díaz AI, Hernandez-Cuevas FJ, Aleman M, Hernandez-Como N (2011) Photoluminescence and Raman scattering in Ag-doped ZnO nanoparticles. *J Appl Phys* 109:014308. <https://doi.org/10.1063/1.3530631>

Publisher's Note Springer Nature remains neutral with regard to jurisdictional claims in published maps and institutional affiliations.